RESTING STATE CONNECTIVITY IN THE RAT BRAIN

A Thesis
Presented to
The Academic Faculty

By

Kathleen Anne Williams

In Partial Fulfillment
Of the Requirements for the Degree
Master of Science in Bioengineering

Georgia Institute of Technology

December 2006

RESTING STATE CONNECTIVITY IN THE RAT BRAIN

Approved By:

Dr. Shella D. Keilholz, Advisor
Department of Biomedical Engineering
Georgia Institute of Technology and Emory University

Dr. Xiaoping Hu
Department of Biomedical Engineering
Georgia Institute of Technology and Emory University

Dr. Donald G. Rainnie
Department of Psychiatry
Emory University School of Medicine

Date Approved:
November 2, 2006

ACKNOWLEDGEMENTS

This work could not have been completed without the assistance and input of many colleagues in BITC. First and foremost, my advisor Shella Keilholz has been a great resource for her own knowledge as well as guidance when we were both unclear on certain directions to take. I only hope I have produced work that she can be proud of as well. Stephen LaConte and Scott Peltier have proven indispensable for data analysis interpretation and processing.

Graduate work has become bearable and enjoyable being surrounded by enthusiastic peers that are always willing to help out or listen to complaints and give some perspective. This group spans from my one-and-only labmate (so far), to the students in the BITC lab, to other Georgia Tech graduate students.

I would like to thank my thesis committee for input that is included in this work, as well as improvements for my future work. Special acknowledgements go to the Laboratory of Functional and Molecular Imaging, National Institutes of Health for use of their 11.7 T MRI system.

Finally, I deeply thank my family and friends for constant support and encouragement.

TABLE OF CONTENTS

LIST OF TABLES

LIST OF FIGURES

SUMMARY

Functional MRI is a method of imaging changes in blood oxygenation that accompany neural activity in the brain. A specific area within fMRI studies investigates what the brain is doing when it is not being stimulated. It is postulated that there are distinctly separate regions of the brain that are connected based upon functional relations and that these connected regions synchronously communicate even during rest. Resting state connectivity has become a tool to investigate neurological disorders in humans without specific knowledge of the mechanisms that correlate neural activity with brain metabolism and blood flow. This work attempts to characterize resting state connectivity in the rat brain to establish a model that will help elucidate the relationship between functional connectivity, as measured with fMRI, and brain function. Four analysis techniques, power spectrum estimation, cross correlation analysis, principle component analysis, and independent component analysis, are employed to examine data acquired during a non-stimulation, single-slice, gradient echo EPI sequence in search of functionally connected, spatially distant regions of the rat brain.

1 INTRODUCTION

1.1 fMRI Background

The technology of functional brain imaging has made significant progress over the course of the last thirty years, from metabolically-based images derived from PET scans to high speed monitoring of the electrical activity of neurons using electroencephalography. This advance in technology is not without strong reason. The brain is the most complex structure in the known universe. It comprises two percent of the weight of the human body, and yet it consumes 20% of the body's blood oxygen supply. The brain governs emotion and physiology of the whole body, but the mechanisms by which it does so are not clearly understood.

Knowledge about the brain has taken many steps throughout history. Ancient Egyptian texts hold the first mention of the human brain in the context of people with head injuries. Brain anatomy and physiology has since been studied to reveal structure and function. Imaging modalities such as computed tomography (CT) and magnetic resonance imaging (MRI) have opened a window into capturing pictures of living brains. Functional MRI (fMRI) has turned those pictures of living brains into movies. Functional imaging is a very powerful and important tool for deciphering the mechanisms of the brain. Medicine and histology may have established the physical brain regions and pathways, but how does the brain go about doing what it does, and just what does it do? These are questions that current research still struggles to answer, and fMRI can help.

Functional MRI is a method of imaging changes in blood oxygenation that accompany neural activity in the brain. Through rapid image acquisition and adjustment of parameters, contrast of MR images can change over the course of a few minutes based on the magnetic properties of blood. This imaging technique allows researchers to noninvasively gather information about the brain in a fourth dimension: time. FMRI can then be used for countless experiments to decode what happens in the brain during specific tasks under varying conditions or influences. FMRI is a research tool used in psychology, psychiatry, neurology, and neuroscience, and proves to illustrate that a working knowledge of how the brain functions is still in progress.

In order to deduce information about brain function using fMRI, researchers design paradigms that consist of periods of stimulation within an imaging timeframe. The stimulation periods produce activity in the brain, which then prompts a series of physiological events. Neural activity induced by stimulation triggers metabolic activity because of energy requirements, which in turn prompts blood blow. Changes in blood flow and blood oxygenation cause a change in the MR signal being acquired because of the difference in magnetic properties between oxygenated blood and deoxygenated blood. Thus, a chain of correlated events, from neural activity to metabolism to blood flow to signal changes, allows researchers to study brain function.

A more specific investigation within fMRI studies aims to ascertain what the brain is doing when it is not actively engaged in any specific activity, that is, when the brain is not being stimulated. It is postulated that there are distinctly separate regions of the brain that are connected based upon functional relations and that these connected regions synchronously communicate even during rest. For example, data analysis shows that

signal time courses from areas of the brain associated with motor tasks correlate even when the individual being imaged is not doing a motor task. Is there a consistent hand-shake interaction between neurons involved in specific networks? As we learn more about the brain, more questions surface.

Specific challenges accompany studying resting state functional connectivity because, rather than comparing two states, stimulation versus rest, based on a pre-designed paradigm, there is no expected time course of activity. The challenges can be managed with appropriate data analysis techniques, as will be addressed in this work.

1.2 Motivation

The implications and assumptions surrounding fMRI and functional connectivity in particular are significant in neuroscience and carry much clinical potential. A search on PubMed for "functional connectivity" results in over 1,700 articles, and the concept is not yet two decades old. Functional connectivity is a statement about observed correlations and does not imply how correlation is mediated [1]. It is known that hemodynamics are being imaged, and some studies have backed up evidence with alternative modalities such as EEG, but it is not clear how tightly hemodynamics are coupled to neural activity, nor what underlying activities govern these changes when the brain is supposedly "at rest." The MR signal fluctuations of resting brain activity that led to functional connectivity investigations are clearly following functional neuroanatomy and not vascular territories, but it is not known why. There are intrinsic limitations of investigating the underlying physiological mechanisms of functional connectivity in humans. While some preliminary explorations have begun, functional connectivity has not been studied extensively in rodents, and yet rodents are often used in research as

human analogs. Rodents have well-characterized brains, and the use of rodents in scientific studies allows more freedom for investigation, such as the ability to probe neural networks through the use of behavioral and biochemical techniques [2]. Extension of functional connectivity studies to the rodent would enable a more thorough investigation into this phenomenon.

1.3 Goals

This work attempts to characterize resting state connectivity in the rat brain to establish a model that will help elucidate the relationship between functional connectivity and brain function. Four analysis techniques are employed to examine data acquired during a non-stimulation imaging sequence in search of functionally connected, spatially distant regions of the rat brain.

1.4 Organization of the Thesis

This document has been organized in a manner thought best to help build the many layers of knowledge and assumptions involved in functional connectivity. After the introduction, which contains the motivation and goals of this research, a background is provided. The background presents a brief description of the physics involved in any MRI technique as well as that which is used for the fast imaging techniques used in fMRI. The second portion of the background lays the basis of functional imaging, resting state, and the implications of functional connectivity in a scientific context. The theory and methods section explains the data analysis techniques applied in this research and outlines the steps of the research from image acquisition to processing and analysis. Results are presented and discussed in the fourth chapter of the thesis, and the final

chapter sums up conclusions of the research presented in the thesis.

2 BACKGROUND

2.1 MRI Physics

2.1.1 A Brief History of MRI

A quick explanation of the foundations of MRI illustrates the capacity of growth of a relatively simple concept into a technology as complex as the discipline of magnetic resonance imaging. In 1952, Bloch and Purcell were jointly awarded the Nobel Prize in physics for their individual work with hydrogen nuclear proton spins and their interaction with a magnetic field [3, 4]. They detailed experiments and theories behind measuring the precessional signal from a spinning proton in water and paraffin, thus the beginning of nuclear magnetic resonance (NMR). Ernst furthered work with the NMR signal through application of the Fourier transform to gain NMR spectra, which he presented in 1966. He followed that presentation with inspiration from Lauterbur's work, imaging using gradient pulse and phase encoding [5].

MR imaging has its origins in the work of Lauterbur reported in 1973. His imaging theory was based on the accepted concept of the intrinsic angular momentum of a proton rotating at the Larmor frequency in an external magnetic field. Lauterbur demonstrated that frequency components of the NMR signal could be spatially encoded, and proposed that if spatially variant magnetic fields were imposed upon an object, its proton spins would deviate from Larmor frequency accordingly, thus allowing spatial information to be

extracted from the frequency data of the NMR signal [6]. Soon afterwards, Mansfield employed fast scan proton density imaging using spatial encoding [7]. From these steps in science stemmed the beginnings of magnetic resonance imaging.

2.1.2 MRI Spin Physics

To gain insight into the basis of MR image acquisition, a brief explanation of MRI physics is in order. MRI begins with the proton spin of a hydrogen nucleus, usually that of water in the body, and its interaction with an external magnetic field, B_0. Figure 2.1 allows better visualization of this interaction.

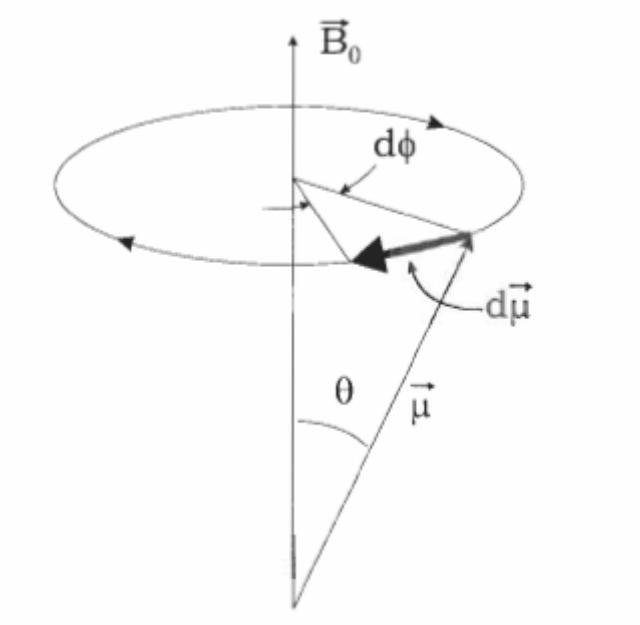

FIGURE 2.1: Proton spin in a magnetic field [8]

The proton spin possesses a magnetic dipole moment vector, μ, which tends to align itself with the static external field, B_0. The interaction of the magnetic moment and B_0 causes instantaneous rotation of the moment about the field. A proton's tendency toward alignment with B_0 is compromised by thermal energy, and an angular component

is introduced, leading to a precession angular frequency known as the Larmor frequency, ω_0. The Larmor frequency is the product of the external field and the gyromagnetic ratio, γ that is equal to 42.6 MHz/Tesla. Operation of the MRI system is based on the fundamental Larmor frequency; for example a 3 T magnet induces spins in the body to precess at 127.8 MHz. The frequencies of the spins are then manipulated through the rest of the MRI system to deviate from Larmor frequency for magnetization detection and image acquisition.

From a quantum physics perspective, the angular momentum of protons can be described in a discrete fashion in which a proton is either parallel or antiparallel to the magnetic field. The position of alignment is heavily affected by absolute temperature, T. The number of spins that are parallel to the magnetic field, a lower energy position, exceeds the number of spins that are antiparallel, a higher energy position. This difference of spin positions is governed by Boltzmann's equation, and termed spin excess:

$$spin\_excess \cong N\frac{\hbar\omega_0}{2kT} \tag{2.1}$$

where N is the total number of spins in the sample, *k* is Boltzmann's constant, and $\hbar\omega_0$ is the Larmor precession frequency in terms of Planck's quantum constant, $\hbar \equiv h/(2\pi)$. The collective count of spins in a given amount of tissue allows easier visualization of the possibility of magnetic field changes large enough to acquire spatial frequency data. These collective magnetic moments are viewed per units of volume called voxels and referred to as the magnetization vector, $\vec{M}(\vec{r},t)$. Proton spins can be tipped by the application of a radiofrequency magnetic field, or rf pulse, that comes from a nearby

transmit coil. The degree to which the spins are tipped depends upon the duration of the rf pulse applied to the body; the rf pulse is resonant with the proton spins at Larmor frequency, allowing efficient spin manipulation. Tipped spins produce a difference in magnetization that changes the flux in the nearby receive coil. That is, from a voxel perspective, after an rf pulse the magnetization has been altered from a position parallel to the field in which its longitudinal magnetization, $\vec{M}_z$ or $\vec{M}_{\parallel}$ is at equilibrium, $\vec{M}_0$, to a position that includes a combination of transverse magnetization components, $\vec{M}_x$ and $\vec{M}_y$, or $\vec{M}_{\perp}$. The concepts of longitudinal and transverse magnetization lead to the introduction of the set of governing equations upon which the principles of image acquisition are based, the Bloch equations. [8]

2.1.3 Relaxation times and the Bloch Equation

The Bloch equation and its cross product components describe the rates at which transverse magnetization, that in the x and y directions, returns to longitudinal magnetization, that in the z direction. The signal acquired in magnetic resonance imaging is based upon the Bloch equation.

$$\frac{d\vec{M}}{dt} = \gamma\vec{M} \times \vec{B}_{ext} + \frac{1}{T_1}(M_0 - M_z)\hat{z} - \frac{1}{T_2}\vec{M}_{\perp} \tag{2.2}$$

The motion of the magnetization vector is described above in terms of each direction component relative to the main magnetic field, $\vec{B}_{ext} = B_0\hat{z}$. The relaxation terms T_1 and T_2 will be explained shortly. The differential equations derived from the calculation of the

components of the cross product above yield solutions from which relaxation times and the MR signal can be calculated.

$$M_x(t) = e^{-t/T2}(M_x(0)\cos\omega_0 t + M_y(0)\sin\omega_0 t) \quad (2.3)$$

$$M_y(t) = e^{-t/T2}(M_y(0)\cos\omega_0 t - M_x(0)\sin\omega_0 t) \quad (2.4)$$

$$M_z(t) = M_z(0)e^{-t/T1} + M_0(1-e^{-t/T1}) \quad (2.5)$$

Image signal characterization is often communicated through the phase of the complex representation of the magnetization solutions of the Bloch equation. The complex representations of the solutions are as follows:

$$M_+(t) \equiv M_x(t) + iM_y(t) \quad (2.6)$$

$$M_+(t) = M\perp(t)e^{-i\varphi(t)} \quad (2.7)$$

The combined effects of transverse magnetization decay and longitudinal magnetization regrowth after a 90° pulse is shown in Figure 2.2 below.

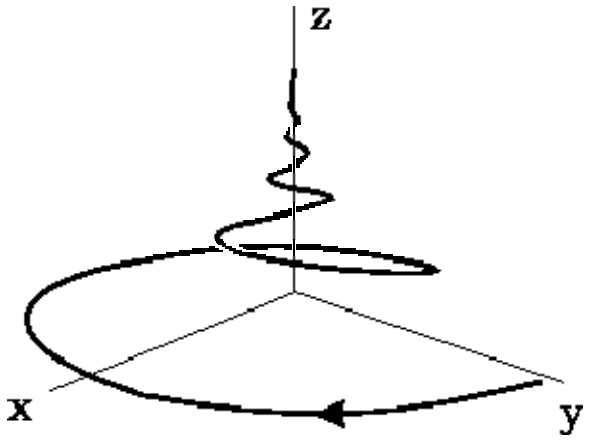

FIGURE 2.2: Transverse magnetization decay and longitudinal magnetization regrowth [8]

To clarify the meaning of the prior equations as well as the concepts of magnetization decay and regrowth, an explanation of relaxation terms is in order. In the presence of the static external magnetic field, any disturbance of longitudinal magnetization into transverse magnetization through the application of an rf pulse is soon recovered by the protons' tendency to realign with the static field, which is its lowest energy position, M_0. This interaction between the proton and its surrounding neighborhood lattice can be described through the rate of change of longitudinal magnetization, $dM_z(t)/dt$, which is proportional to the proton's deviation from equilibrium, $M_0 - M_z$. Multiplication of this difference with an empirically determined constant, the inverse of the "spin-lattice" relaxation time, yields an equation that describes growth of longitudinal magnetization of a proton.

$$\frac{dM_z}{dt} = \frac{1}{T_1}(M_0 - M_z) \qquad (\vec{B}_{ext} \parallel \hat{z}) \qquad (2.8)$$

This first-order differential equation can be seen as a component of the Bloch equation (2.2). The relaxation parameter T_1 depends upon the tissue being imaged, and allows for image contrast. T_1 is on the order of tens to thousands of milliseconds, depending upon the specific tissue and the B_0 field. Another relaxation parameter dependent upon the subject of imaging is T_2, "spin-spin" relaxation time, which describes the reduction of transverse magnetization. The fanning out of individual spins that have been tipped simultaneously but each feel a different local field through interaction with each other as well as the applied field is known as dephasing, which reduces transverse magnetization. The decay term in the differential equation describing the movement of transverse magnetization accounts for spin-spin relaxation.

$$\frac{d\vec{M}_{\perp}}{dt} = \gamma \vec{M}_{\perp} \times \vec{B}_{ext} - \frac{1}{T_2}\vec{M}_{\perp} \tag{2.9}$$

Often in MR physics, a rotating laboratory frame is utilized to better visualize proton movement in reference to the Larmor frequency upon which the theory is based. In the rotating frame, the rf pulse that has a frequency matched to the Larmor frequency is then seen as tipping spins at specific angles, for example 90° or 180°. Figure 2.3 demonstrates the dephasing of a set of spins tipped at a 90° pulse, as well as the total magnetization, in the laboratory frame.

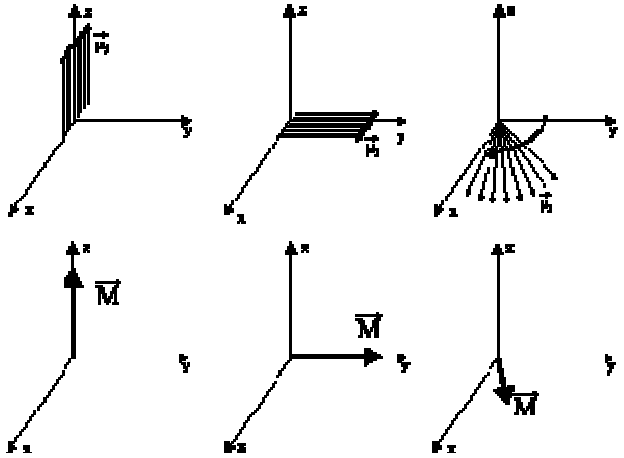

FIGURE 2.3: Transverse magnetization dephasing and decay [8]

T_2 is usually shorter than T_1, most often in tens of milliseconds in human tissue, but has a large range between solids (microseconds) and liquids (seconds). Another dephasing term necessary to account for magnetic field inhomogeneities is T_2*, a relaxation time which accounts for both internal and external field inhomogeneities affecting transverse magnetization decay.

$$\frac{1}{T_2 *} = \frac{1}{T_2} + \frac{1}{T'_2} \tag{2.10}$$

The intrinsic components of T_2* are related to local, random, time-dependent field variations. The magnitude of signal associated with T_2* can be modeled as an exponential function of position in the magnet, r, and time, t,

$$M\perp(r, t) = M\perp(r, 0)e^{-t/T2*} \tag{2.11}$$

This magnetic susceptibility, though generally considered a nuisance in imaging, becomes the basis of applications of functional MRI, as will be explained further. [8]

2.1.4 MR Image Acquisition

Through the application of spatially varying magnetic field gradients in the x, y and z directions, the magnetization of the subject being imaged can be manipulated with rf pulses. The magnetization relaxation produces a signal with spatially varying frequency components that is detected by the nearby receive coil. Voltage data is collected from the receive coil by sampling of the signal with an analog-to-digital converter ADC. Inverse Fourier transformation of the signal allows us to elicit spatial data that can then be demodulated, reconstructed and rendered into an image.

The collective signal acquired prior to Fourier transformation is referred to as k-space data. The use of gradients to allow movement across k-space is known as frequency encoding. A gradient applied in the x direction, the readout gradient, the y direction, the

phase encoding gradient, and the z direction, the slice-selection gradient, can cover a plane of k-space. ADC sampling occurs during application of the readout gradient.

There are many rf and gradient pulse sequences used each for their own purpose of weighting an image with T_1 or T_2 relaxation, or a combination, depending on the necessities of the application. Our particular application of functional MRI uses a method of imaging called echo planar imaging, or EPI. EPI is a fast imaging technique in which, after a single rf excitation, a train of "echoes" that refocus transverse magnetization are applied in the readout direction. Between each echo, a blip in the phase encoding direction moves the readout to a new line of k-space. This allows the acquisition of an entire slice of k-space data in one repeat time T_R, which is one cycle of rf pulse and ADC sampling. Echo time T_E is an important parameter used to measure when refocusing of the signal occurs. Figure 2.4 below is a sequence diagram that shows the gradient application in an EPI sequence.

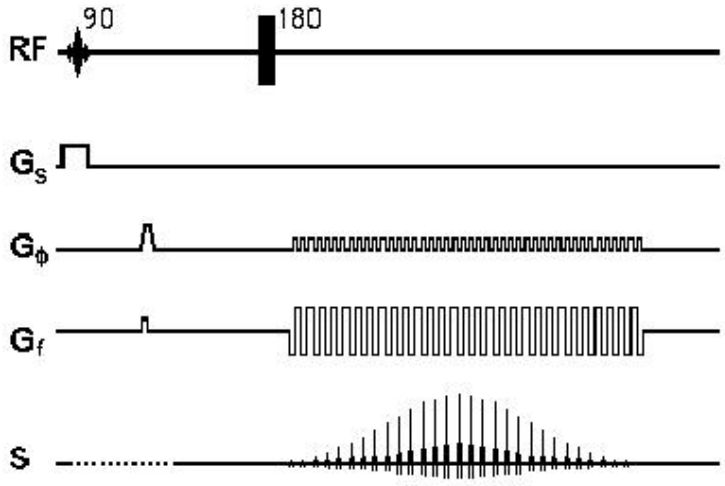

FIGURE 2.4: Spin echo EPI pulse sequence

It is important to take into consideration the compromise between time and resolution for such a fast signal acquisition method. In order to obtain a signal before complete dephasing of the transverse magnetization, sampling is limited to the length of T_2*. [8]

2.1.5 T_2* and the BOLD Effect

As mentioned earlier, T_2* exhibits magnetic susceptibility due to local, random, and time-dependent field variations. A component of local field variation in T_2* can be explained through the paramagnetism of deoxygenated blood. Deoxyhemoglobin contains unpaired electrons that influence the phase of the signal of the blood volume. The magnetic properties of blood make deoxyhemoglobin a naturally occurring contrast agent for MRI and open a window for investigation of blood-oxygen consumption in the brain. Oxyhemoglobin is diamagnetic, which does not influence the MR signal, but the presence of paramagnetic deoxygenated blood particles causes more dephasing of the protons, so the MR signal is influenced by susceptibility changes between the two blood states. Increased blood flow to a region accompanies regional activity, causing changes in MR signal in areas of increased brain activity. This phenomenon is called the BOLD effect for blood oxygenation level dependence. Changing T_2* is reflected in signal change during imaging, thus making BOLD a powerful tool for imaging brain function [9]. During brain activity, metabolism increases, leading to an increase in bloodflow. The proportion of oxyhemoglobin to its deoxygenated counterpart is greater with the surge of new blood, leading to longer T_2* and a greater MR signal. BOLD imaging captures the activities of local vasculature of the brain that are coupled with neural activity, but the exact mechanism or relationship between the two functions is not clearly understood.

2.1.6 High Field and Small Animal Imaging

A determining factor of the quality of image acquisition is the signal-to-noise ratio (SNR), which can be improved with higher magnetic field strength. While typical human scanners are 1.5 T or 3 T, higher field magnets can be used to obtain greater signal and higher resolution images. To increase SNR, higher-field magnets are often used for small animal imaging. In 1996, Huang et al demonstrated great enhancement of fMRI signals through the use of a 9.4 T MRI system on mice during visual stimulation with flashing lights [10]. Temporal differentiation was facilitated because the BOLD signal enhances linearly with higher-field imaging systems [11]. Image acquisition for our studies was conducted in an 11.7 T scanner and a 9.4 T scanner. During stimulation, BOLD signal fluctuations in 11.7 T constitute 6-8% of the signal change. The use of small animals for scientific models is valuable in the sense that many parameters can be manipulated physiologically, such as genetic knockouts, brain lesions, and tumor placement. Also, more invasive measurement techniques can be used like electrophysiology. This constitutes much of the motivation behind characterizing resting state connectivity in rats.

2.2 fMRI

2.2.1 Functional Brain Imaging Modalities

The brain is quite obviously the center of operations of the body, but the mechanisms by which it does so are poorly understood. Functional imaging has become a powerful tool in the efforts to demystify way the brain works. There are several modalities with which brain activities are measured or viewed. Electroencephalography (EEG) measures the

electrical activity of the brain by recording from electrodes that are placed on the scalp. The measurements of the EEG are of voltage differences between different parts of the brain; these voltage differences are representative of the electric signal elicited from postsynaptic potentials of large numbers of neurons. EEG has the benefit of a high temporal resolution, on the order of milliseconds, but is generally only a surface measurement of brain activity. Magnetoencephalography (MEG) measures magnetic fields produced by electrical activity in the brain using superconducting quantum interference devices (SQUIDs) that can detect magnetic fields as small as femtoteslas ($1fT = 10^{-15}$ T). MEG measurements represent net ionic currents flowing in dendrites of neurons during synaptic transmission as well as activity in extracellular fluids, but cannot measure the activity produced by action potentials because of the reverse activity involved in action potential kinetics [12]. Near infrared spectroscopy (NIRS) utilizes the oxygenation-dependent variation of the hemoglobin absorption spectrum to measure localized changes in regional blood flow that occur with neural activity [13]. NIRS can measure deeper into a sample than EEG or MEG, but in order to penetrate three-dimensionally into the brain, more involved and expensive techniques like PET and MRI are necessary.

Positron emission tomography (PET) is a nuclear imaging technique in which positrons are used for labeling of tracers that are taken into the body. Once inside the body, positrons travel a short distance then collide and annihilate with nearby electrons. After annihilation, two photons are emitted in opposite directions whose scintillation is detected by coincidence detectors. Reconstruction of the detected positron activity allows three-dimensional images to convey information related to metabolic brain activities and blood flow. Particular radio-labeled tracers are used for particular measurements; PET isotopes can be labeled to most organic molecules. For example,

^{18}F-labeled deoxy-2-fluoro-D-glucose (^{18}F-FDG) can be used to quantify regional cerebral glucose utilization, which usually correlates with regional synaptic activity. ^{15}O-labeling can help to measure regional cerebral blood volume (rCBV) or regional cerebral blood flow (rCBF) using ^{15}O-CO and ^{15}O-H_2O, respectively. ^{15}O-labeled tracers are commonly used in stimulation studies. The concept of stimulation studies will be further explained later. Cerebral activation patterns can be measured with image subtractions. PET is also being used with labeled ligands in order to visualize receptor binding parameters, which can be detected on a pixel-by-pixel basis. PET images allow absolute quantification through signal detection. Single-photon emission computed tomography (SPECT) is a nuclear medicine application that utilizes rotating gamma cameras that detect gamma rays emitted by radionuclides inside a patient. Tomographic images can be reconstructed to show three-dimensional information in cross-sectional images. Brain perfusion, benzodiazepine receptors, dopamine-D2 receptors, and protein metabolism can all be imaged with use of particular radiopharmaceuticals; a commonly used tracer label is ^{99m}Tc. SPECT images allow "freezing" of a brain state immediately after perfusion tracer injection so the brain scan can occur hours later; this proves to be very useful in sleep studies [14, 15].

MRI introduces several more noninvasive modalities by which brain function can be measured. Functional MRI (fMRI) is a special term that refers to MR imaging modalities based on brain activation. Three very telling measurements of brain activity that can be facilitated through the use of MRI are regional cerebral blood flow, regional cerebral blood volume, and blood oxygenation level. Arterial spin labeling (ASL) can map rCBF using magnetic spin labeling of a particular slice in the brain, in which spins of the protons outside the imaging slice are tagged with an rf pulse, time for perfusion is allowed, and the slice is imaged. Subtraction of this tagged image from a control image

shows perfusion information about the region of interest [16]. rCBV is often imaged using exogenous contrast agents, like iron oxide, that alter relaxation times in the blood, thus increasing image sensitivity to blood volume changes in the brain vasculature. Blood oxygenation can be visualized using BOLD imaging techniques, as has been mentioned previously and is the basic methodology utilized in this study.

2.2.2 Experimental Paradigms

Stimulation paradigms are commonly used in functional neuroimaging experiments and are a way to distinguish different brain activation patterns. During stimulation, the brain is said to be in an activated state, and conversely, when there is no stimulation the brain is said to be deactivated or at rest. Correlation among areas in the brain is then determined through a chosen post-processing technique, usually through cross correlation of the signal time course data with a box-car function that resembles the stimulation paradigm. Stimuli in functional neuroimaging are based upon the parameters of interest and can be assigned tasks or presented events. Finger-tapping, visual stimuli, word association tasks, and scents are all examples of stimuli that can elicit activation in the desired area of the brain. Stimulation in fMRI experiments is generally designed based upon the time course of BOLD signal evolution, which is referred to as the hemodynamic response function (HRF). The HRF lasts about 10-15 seconds after a brief stimulus. Regional hemodynamics and metabolic activity are tightly coupled to regional neuroactivation [17, 18]. This close relationship increases the value of studying hemodynamics to probe neurophysiological information.

Two broad design classes can sum up the variety of experimental paradigms that are used in functional neuroimaging, blocked designs and event-related designs. Blocked

designs present a single stimulus continuously for an extended period of time, typically 20-30 seconds, longer than the HRF that might result from a single-event stimulus. The additive nature of the HRF then allows any detection of activation to be held attributable to the particular stimulus presented. Event-related designs are discrete presentation of stimulus events that may vary in duration and interstimulus intervals, thus allowing characterization of transient changes in fMRI signals. Event-related designs help eliminate or reduce such confounds as habituation and anticipation. Mixed designs incorporate block-design characteristics as well as event-related characteristics in an effort to garner information of both types [14]. Image processing techniques are heavily influenced by design type and the HRF. Convolution of the stimulus function with the HRF offers a smoother, more realistic fit of the model with physiological data [19]. Since this study focuses on the human brain at rest, there is no delineated paradigm function or prompted hemodynamic response that can be used to investigate underlying causes of change. Processing steps will be further explained in the methods section of this text.

2.2.3 Functional Connectivity in the Human Brain

Recently in fMRI studies, more attention is being paid to the conditions of the human brain at rest, and correlations in brain activity during a deactivated state. In 1995, Biswal et al introduced the concept of functional connectivity in the motor cortex of the human brain during rest detected within fMRI image signals [20]. This study was followed by other groups' studies that revealed evidence of connectivity between additional functional areas of the brain, such as the somatosensory and visual cortices [21-23]. Functional connectivity is a term used to describe synchrony between signals of spatially distinct areas of the cortex [24]. In the introduction of the BOLD effect as a functional imaging tool, Ogawa subtly noted observations of MR signal intensity fluctuations of

about 2% in the brain during periods of rest [9]. Fluctuations in the lower frequencies, that is, around 0.08 Hz, are presumed not to be associated with system noise or cardiac or respiratory peaks. Biswal analyzed the low-frequency fluctuations (LFF) in pixels from the motor cortex of a resting human brain and found temporal correlations among them and between remote areas also believed to be associated with motor function [20]. Resting state connectivity has become the subject of myriad studies which may be characterized as going down two paths, those attempting to pin down the physiological mechanisms of low-frequency fluctuations, and those probing into the neuropsychiatric implications of the existence of a resting state network.

2.2.4 LFF and Confounding Artifacts

There are several criticisms of the theory of functional connectivity, namely in the source of the low-frequency fluctuations. By examining individual noise contributions to the MR signal through variations in flip angle and echo time, Kruger and Glover demonstrated the dominance of physiological noise in the T_2*-weighted signal [25]. This study helped quiet arguments that signal fluctuations are system-dependent and promoted the investigation of the noise. The actual physiological mechanisms of the LFF are not clearly understood, and some protests have posited that the fluctuations are actually higher frequency physiological events that are being aliased into the lower frequencies. Biswal imaged the BOLD signal using EPI as well as blood flow using ASL in a functional connectivity study, and found the magnitude of the LFF to be higher in BOLD-weighted images than in flow-weighted images, suggesting that LFF are more closely associated with neurophysiological activity rather than vasomotion [26]. A study of anesthetized children in which two sampling rates were used revealed a consistent peak in a very low frequency of the power spectrum. This study verified that BOLD signal

fluctuation in low frequencies is not aliased physiological noise [27]. Numerous studies have incorporated EEG, MEG, and PET among other tools to investigate theories that the LFF originate from neuronal activity, CBF, CBV, metabolism, or some other phenomenon [23, 24, 28, 29]. A major concern, especially in animal studies, is the use of anesthesia during imaging and how that affects LFF. Depending on the type of anesthesia and its effects on vasomotion, interregional functional connectivity can be enhanced or abolished [26, 27, 30].

2.2.5 Resting State Networks and the Default Mode Hypothesis

Assumptions of functional interdependence based upon the LFF of fMRI have become motivation to characterize the MR signal more specifically. Characterization of the spontaneous fluctuations can then lead to physiological explanation. Cordes et al used spectral decomposition of correlation coefficients to illustrate which frequencies contribute to interregional connectivity and show that these contributing frequencies are all less than 0.1 Hz [21]. Later, the same group demonstrated that resting state maps acquired from the major frequencies contributing to functional connectivity closely resembled task-activation maps of auditory, visual, and sensorimotor regions [31]. Using PET studies of the brain oxygen extraction function (OEF), or the ratio of oxygen used by the brain to oxygen delivered by flowing blood, Raichle et al investigated observations of task-induced decreases in regional brain activity. These investigations resulted in the proposal of an organized mode of brain function that is present as a baseline or default state and is suspended during goal-oriented behaviors [32]. Activity attenuation in task-independent areas of the brain spur further theories of what the default mode might suggest about its own mechanisms [33]. The list of potential contributing factors continually evolves as do their implications. Possible explanations

include a dynamic interaction between cognitive processes and the emotional state of the subject, self- versus externally-focused attention, or modulation of brain activity to prevent unpredictable variation of activity [32, 34]. Based on the assumption that regions whose BOLD signal fluctuations show a high degree of temporal correlation constitute a tightly coupled neural network, it has been shown that there is at least one widely-distributed network within the brain that decreases in activity during task performance [35]. The speculation of a single resting state default brain mode has given way to investigations of task-positive and task-negative anticorrelated sets of brain regions as well as multiple resting state networks (RSN) [36, 37]. Employing "model-free" methods of data analysis rather than the commonly utilized cross correlation analysis reveals evidence of as many as five RSNs. Across subjects, five spatiotemporally distinct patterns of low-frequency coherences across long distances in the brain were shown using probabilistic independent component analysis (PICA) and interpreted to be associated with functionally integrated regions [37]. These distinct regions are illustrated in figure 2.5 below and were found to be physiologically connected using diffusion tensor imaging (DTI) which shows white matter tracts in the brain, and perfusion.

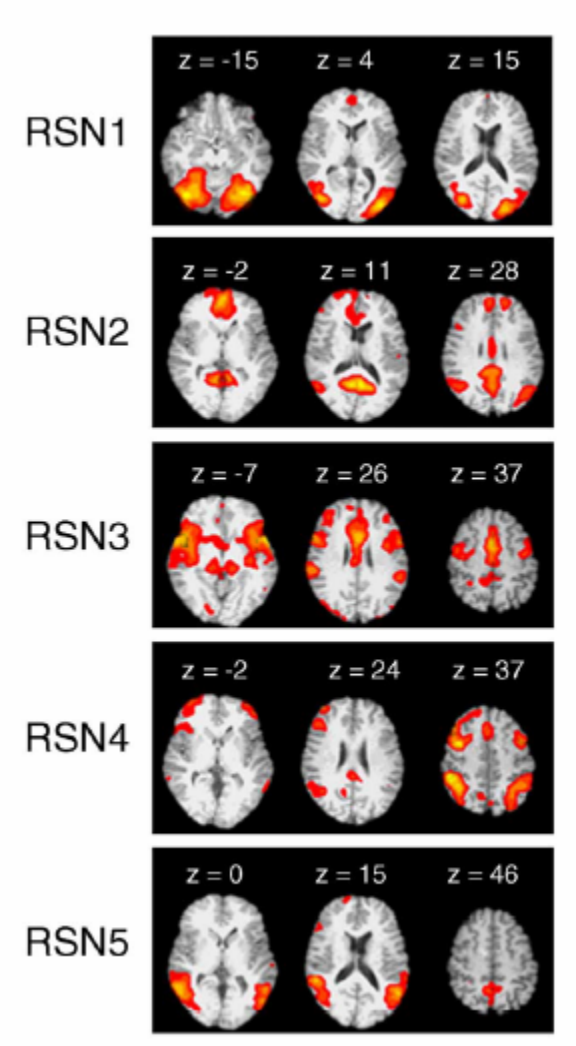

FIGURE 2.5: Illustration of five resting state networks identified by De Luca et al [37]

2.2.6 Integration of Neurology, Psychiatry, and Neuroscience

As theories surrounding the mechanisms of resting state functional connectivity grow closer to self-awareness and modulation of baseline activity, the ties between the once somewhat distinct disciplines of neurology, psychiatry, and neuroscience bind tighter. The research of neuropsychiatric disorders such as Alzheimer's disease and schizophrenia, among others, entails studies of reduced connectivity or incoherencies in transitions between default and task-oriented modes of brain activity [38, 39]. The

implications of resting state networks and the possibility of monitoring an individual's introspection or self-regulation can tremendously impact diagnosis and treatment of neuropsychiatric disorders.

Functional neuroimaging has become a powerful tool in evaluating the specific disorder behind these diseases, and functional connectivity shows promise of discovering details of brain pathophysiologies. It is important to characterize low frequency fluctuations in the human brain in the resting state and to identify their underlying physiological mechanisms. The ability to trace hemodynamics of deactivated brain networks back to a neuronal basis can further establish the use of functional MRI as a diagnostic tool. Certain limitations accompany the study of humans when the physiology of a particular action is unclear. Studying humans with diagnosed disorders showing reduced connectivity and humans under anesthesia can help delineate some details of the mechanisms of LFF, but an animal model can accelerate the investigation. Thus, the motivation behind this study is highly justified in that once resting state connectivity can be demonstrated in a rat and LFF can be characterized, a useful probe into the physiological mechanisms of functional connectivity will be revealed.

3 THEORY AND METHOD

3.1 Theory

3.1.1 Power Spectral Density Estimation

Often used in conjunction are cross correlation techniques and spectral analysis through fast fourier transformation or power spectral density (PSD) estimation. The time courses from regions of high synchrony are separately inspected to ensure correlations are due to fluctuations in the low frequency region of the spectrum. The PSD provides a frequency domain description of a time series, allowing easy detection of outstanding contributions to the time series. For example, the power spectrum of a time series generated near the ventricles of the ventilated rat brain will have a prominent peak at about 1 Hz, the ventilation rate. It is expected that PSD estimations within the somatosensory cortex will show peak structure in the low frequencies. The power spectrum is calculated from the discrete-time Fourier transform of the time series $r_x(k)$:

$$P_x(e^{j\omega}) = \sum_{\infty} r_x(k) e^{-j\omega} \tag{3.1}$$

Estimating the power spectrum is equivalent to estimating the autocorrelation of a process. Because of limitations involving infinite amounts of data with the Fourier transform and noise corruption, there are many techniques with which to estimate PSD. Welch's Method is employed in this functional connectivity application. Welch's Method involves overlapping sequences resulting from data windows applied to the time series. Modified periodograms are then averaged for an estimate:

$$\hat{P}_x(e^{-j\omega}) = \frac{1}{KLU}\sum_{i=0}^{K-1}\left|\sum_{n=0}^{L-1} w(n)x(n=iD)e^{-j\omega}\right|^2 \quad (3.2a)$$

$$U = \frac{1}{L}\sum_{n=0}^{L-1}\left|w(n)\right|^2 \quad (3.2b)$$

where K represents the number of sequences that cover the set of all data points, D is the set of overlapping points, and *w*(n) is the L-point data window [40].

3.1.2 Cross Correlation Analysis

Initially, the primary statistical approach to functional connectivity studies was cross correlation. Cross correlation analysis begins with selecting a voxel or a seed of voxels from a desired area of the brain in the image sequence. Averaging a set of voxel time courses has been found to improve consistency in functional connectivity maps [21]. The time course associated with that seed is then cross correlated with each time course of each pixel in the brain. A two-dimensional matrix of correlation coefficients results from the computation. The correlation coefficient for two time series is a ratio involving their covariance:

$$(t_1, t_2) = \frac{C(t_1, t_2)}{\sqrt{C(t_1, t_1)C(t_2, t_2)}} \quad (3.3)$$

In which $C(t_1, t_2)$ is the covariance of the normalized series:

$$C(t_1, t_1) = \sum_i \sigma_i^2 e^{j\omega(t_1 - t_2)} - \eta(t_1)\eta^*(t_2)\,\mathrm{C}(t_1, t_1) \quad (3.4)$$

With variance σ_i^2 and mean $\eta(t_1)$. The cross correlation function is also referred to as the coherence function [41].

The matrix can then be mapped to reveal a spatial view of correlation, or statistical significance can be calculated using the correlation coefficients. Using a voxel from a ROI in the same dataset allows analysis without making assumptions about the expected temporal outcome, as is the case for task-related data correlated with a specific function. Cross correlation is suitable for fast screening of fMRI data, but there are a number of disadvantages associated with this type of analysis. Assumptions must be made about the expected network so as to select voxels from appropriate regions. The outcome is heavily dependent upon seed selection, which may vary from user to user, or brain to brain. Some groups have employed inspection of each time course within the brain to correlate the most appropriate condition with the rest of the brain, but this is a time consuming task. Also, the sizes of detected voxel clusters of synchrony have great variability [42].

3.1.3 Principle Component Analysis and Independent Component Analysis

Principle component analysis (PCA), also called eigenimage analysis in image processing, is a method of calculating and reporting the variance of a dataset in the form of principle components. PCA of fMRI datasets uses singular value decomposition (SVD) to identify a set of orthogonal spatial modes that capture the greatest amount of variance expressed over time. With PCA, one can reduce the dimensions of a dataset by choosing to analyze the set of principle components that contribute the most variance. Dimension reduction is especially helpful in this application, as the masked matrix that represents the brain activity over time can be on the order of 600-800 signals each with 1200-3600 time points. The SVD of a dataset A is calculated as such:

$$A = \mathbf{USV}^T \tag{3.5}$$

The matrices U and V are orthogonal and calculated from the eigenvectors and eigenvalues of AA^T and A^TA, which are square matrices. The columns of V contain the eigenvectors of $A^T.A$ and the columns of U contain the eigenvectors of AA^T. The square roots of the eigenvalues obtained from the products of AA^T and A^TA comprise the columns of S. The diagonal of S is said to be the singular values of the original matrix, A. Each eigenvector represents a principle component, the first of which has the highest eigenvalue, and explains the greatest amount of variance of the data. In fMRI applications, PCA is fundamentally limited because it offers only a linear decomposition of a set of neurophysiological measurements, and the particular set of eigenimages or spatial modes obtained is uniquely determined by biologically implausible constraints. Nevertheless, for large datasets, PCA is a practical way of reducing dimensions for further analysis.

The principle components chosen to explain the dataset are used for independent component analysis (ICA), which is a more appropriate analysis of biological data. A typical ICA model assumes the source signals are not observable, are statistically independent, and are non-Gaussian in nature, all of which are more appropriate requirements than the orthogonality restriction applied in PCA. All of the unobservable signals are assumed to be combined with an unknown but linear mixing process [43]. Because functional connectivity studies look to identify signals that do not have a predicted structure, ICA is an appropriate analysis technique.

The ICA model can be explained in matrix form as such:

$$\mathbf{x} = \mathbf{As} \tag{3.6}$$

where **x** is a linear mixture, an observed random column vector of *n* independent components, and **s** is the random column vector comprising the *n* independent components. The square matrix **A** is the unknown mixing matrix. After estimation of the

matrix **A**, its inverse **W** can be used to calculate the independent components by multiplication:

$$\mathbf{s} = \mathbf{W}\mathbf{x} \tag{3.6}$$

There are several algorithms with which to implement ICA. The unmixing matrix **A** spatially maps each component to corresponding areas. The method used in this study is FastICA, which uses a very efficient method of maximum likelihood estimation after the data is preprocessed through mean-centering and whitening. FastICA is a fixed-point iteration scheme that finds a maximum of the non-Gaussianity of $\mathbf{w}^T\mathbf{x}$. There are four steps involved in the process:

1. Choose a random initial weight vector, **w**.
2. Let $\mathbf{w}^+ = E - E\{g'(\mathbf{w}^T\mathbf{x})\}\mathbf{w}$

   where g(u) = tanh(au), which represents super-Gaussian data.
3. Symmetric decorrelation is employed using matrix square roots:

$$\mathbf{W} = (\mathbf{W}\mathbf{W}^T)^{-1/2}\mathbf{W} \tag{3.7}$$

   where the inverse square root is obtained from eigenvalue decomposition. For whitened data, decorrelation is the same as orthogonalization. This process prevents different vectors from converging to the same maxima.
4. If no convergence, return to step 2.

For more details on the FastICA algorithm, consult Hyvarinen and Oja, 2000 [44].

There has been some change in trends governing the implementation of spatial ICA (sICA) versus temporal ICA (tICA). Figure 3.1 is a visual representation of how matrix orientation determines which type of ICA is used. If the input matrix contains data signals across rows and time samples down columns, spatially independent components

result from ICA. If the matrix is transposed and each signal comprises a new row with time samples across the rows, ICA reveals temporally independent components.

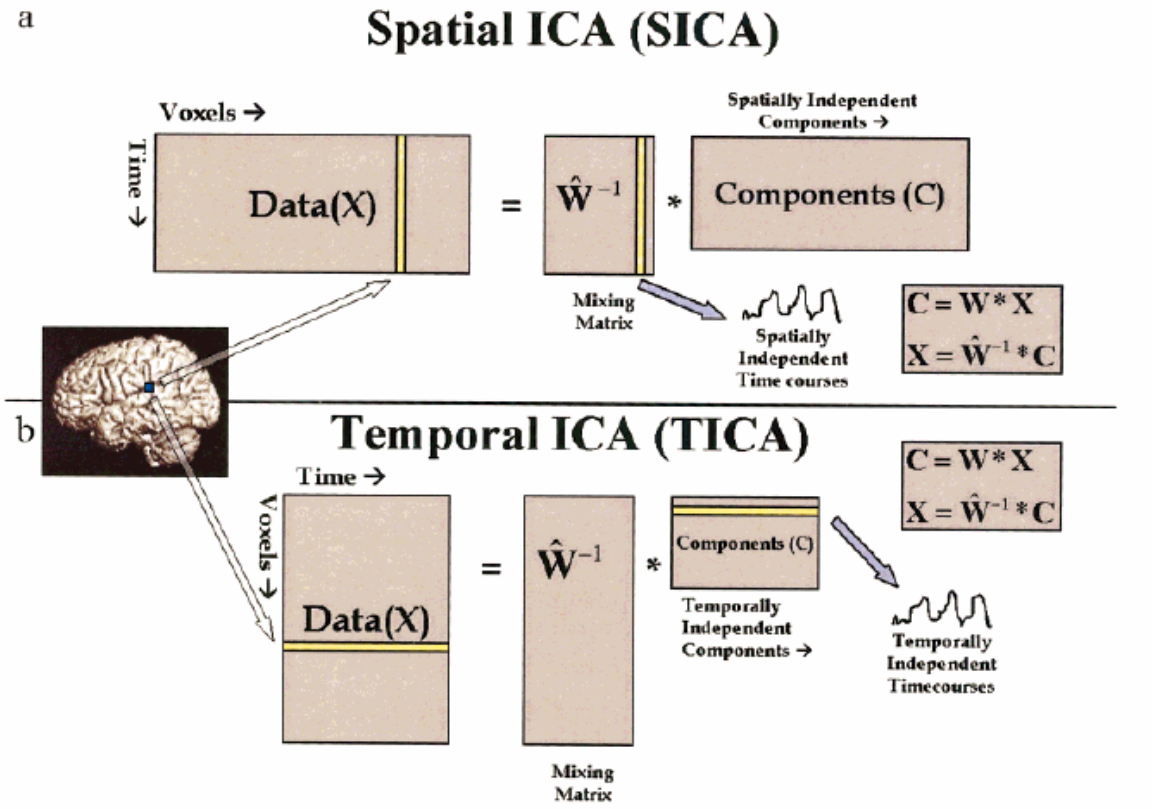

FIGURE 3.1: Graphical illustration of a) spatial ICA and b) temporal ICA [45]

At some point, there was a shift from using tICA to using sICA for fMRI datasets. The greatest reason for this switch is that the spatial dimension is much larger than the temporal dimension of human datasets [45]. Since this is not the case for the current dataset, tICA was implemented.

3.2 Method

3.2.1 Experimental Methods

Six rats were anesthetized with halothane, orally intubated and placed on a mechanical ventilator throughout the surgery and the experiment. Plastic catheters were inserted into the right femoral artery and vein to allow monitoring of arterial blood gases and administration of drugs. After surgery, the rats were each given an intravenous bolus of α-chloralose (80 mg/kg) and halothane was discontinued. Anesthesia was maintained with a constant α-chloralose infusion (27 mg/kg/hr). Paralysis was induced and maintained with pancuronium bromide injections (4 mg/kg/hr). Each rat was placed on a heated water pad to maintain rectal temperature at approximately 37° C while in the magnet. Each animal was secured in a head holder with ear bars and a bite bar to prevent head motion and was strapped to a plastic cradle.

Each rat was imaged on a Bruker 11.7 T scanner using a single-shot gradient-echo EPI sequence to acquire T_2*-weighted MR images. Setup included shimming, adjustments to echo spacing and symmetry, and B_0 compensation. The images were acquired with the following parameters: 64 x 64 matrix, effective echo times (TE) 13, 17, 20, 25, 30, and 35 ms, repetition time (TR) 100 ms, bandwidth 200 kHz, field of view 1.92 x 1.92 cm, with one 2 mm coronal slice covering the bilateral primary somatosensory cortex. Each imaging series consisted of 1200-3600 images of 300 μm resolution. Images were acquired with different echo times to determine optimal sensitivity to the low frequency resting state fluctuations previously seen in human studies. Activation maps were also acquired during electrical stimulation of the forepaw in order to identify the primary somatosensory cortex (SI). A TR of 100 ms allows clear identification of physiological

artifacts such as cardiac or respiratory effects without aliasing into the low frequencies that are of specific concern in this research.

Some data was acquired on a Bruker 9.4 T scanner also with a single-shot gradient-echo EPI sequence and similar setup. Six rats were each anesthetized through a nose cone with a mixture of isoflurane, oxygen, and nitrous oxide. Isoflurane was approximately 5% for induction, then 1.9%, 1.6%, and 1.3% for three subsequent imaging sequences. Each rat was placed on a heated water pad with feedback temperature maintained at approximately 40° C while in the magnet. Each animal was secured in a head holder with ear bars and a bite bar to prevent head motion and was strapped to a plastic cradle. MR images were acquired with the following parameters: 64 x 64 matrix, TE 20 ms, repetition time (TR) 100 ms, field of view 2.56 x 2.56 cm, with one 2 mm coronal slice covering the bilateral primary somatosensory cortex. The image series consisted of 3600 images of 400 μm resolution. Unless otherwise noted, data analysis was conducted with the data acquired from the 11.7 T scanner.

3.2.2 Processing and Analysis

Various preprocessing and analysis techniques were tested, as will be further discussed in Method Optimization in the results section. Most image processing and analysis was performed using Matlab, unless specified otherwise. Motion correction was not performed on any image set because the rats were anesthetized, paralyzed, and properly secured in the cradle as described in the experimental methods section. The omission of motion correction is beneficial for data analysis, especially with resting state data because sometimes motion correction algorithms introduce false elements of coherence in the signal.

Power spectral density analysis was performed on a user-selected 2 x 2 ROI from the EPI dataset. The ROI was selected by referencing activation maps. The four pixel time courses were averaged together, normalized, and linear trends were removed. The power spectral density estimate was calculated and plotted via Welch's method using the pwelch function in Matlab's signal processing toolbox. Regions of interest were chosen in areas expected to exhibit signals characteristic or devoid of specific physiological artifacts. The areas of focus are the somatosensory cortex, the base of the brain, the sagittal sinus, and outside the brain.

For cross correlation analysis, time courses were low-pass filtered. A 0.14 Hz cutoff frequency was used in order to specifically correlate the low-frequency region of the signal in which spontaneous fluctuations have previously been observed. Also, low-pass filtering removes signal contributions from faster physiological effects such as respiration (~1 Hz) and heart rate (~4-5 Hz). Analysis of the stimulation time series was performed using STIMULATE (University of Minnesota) in which a map was generated from cross correlation of the unfiltered image time course and a boxcar waveform representing the stimulation period. The activation threshold was set at 0.2, and only groups that included at least four activated pixels were considered significant. Activation maps and a Paxinos rat brain atlas were then visually referenced in order to choose a 2 x 2 region of interest (ROI) within the primary somatosensory cortex (SI) from an image from the resting state data set [46]. The time courses from each of the four chosen pixels in the ROI were averaged together after removal of linear trends and normalization through subtraction of the time course mean and division by the standard deviation of the time course. The resulting reference time course was then cross-correlated with each other time course from the entire detrended, normalized dataset. A 64 x 64 matrix of

correlation coefficients were mapped and used for statistical analysis. From the correlation map, user-selected clusters of 4 x 4 pixels within the ipsilateral subcortical, contralateral cortical, and ipsilateral cortical regions of the rat brain were averaged and compared using a student's t-test.

Before performing ICA on resting state data, time series were inspected using STIMULATE to detect any significant transient effects in the imaging sequence due to lack of dummy scans, system instability, etc. Any image series that exhibited initial transience was noted. In Matlab, after data read-in, the corresponding number of transient images in the resting time course were removed. After filtering, a threshold mask of about 15% of the maximum signal intensity was created based upon each pixel's time series average. The threshold mask was then used to index and reshape the passing pixels' time courses into a two-dimensional matrix in which each row represents the time course of one pixel. The matrix in this form allows temporal ICA implementation. Linear trends were removed from the time courses, followed by normalization. PCA and ICA were then performed using a freely available software tool for use within Matlab called FastICA [44]. PCA was used to reduce dimensions of the ICA analysis based upon graphing the components that contribute the most variance to the signal. From the PCA plot, an over 90%-variance-explained criterion determined the number of components to which the data set was reduced. The bar graph resulting from PCA exhibited an immediate drop-off from one component to another, a knee, indicating a greater variance contribution from each prior component; these first components were usually chosen for use in ICA because they represented at least 90% of the total variance. Figure 3.2 shows typical PCA bar graph from a rat dataset that explains the amount of variance associated with each component.

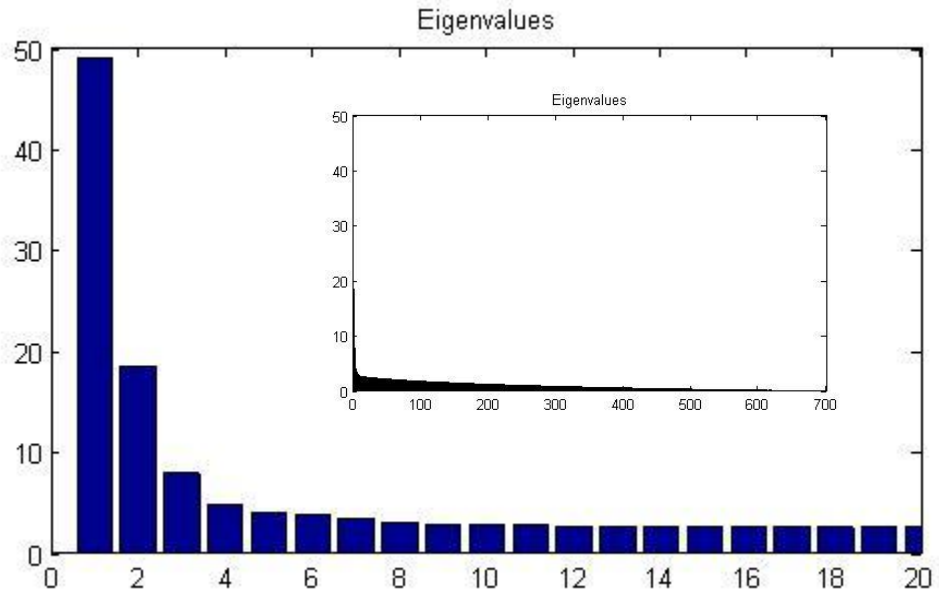

FIGURE 3.2: PCA distribution from FastICA (zoom). Note dropoff between components 2 and 3. Inset: Entire eigenvalue set

The principle components chosen explained over 90% of the data variance, with conditions depending on the specific dataset and the number of components chosen. FastICA automatically whitened the principle components to use for input in the ICA analysis. The independent components were calculated with default FastICA settings, except for the use of tanh as the nonlinearity function, as was followed from another study [42]. Using tanh as a nonlinearity function is suggested in FastICA for super-Gaussian data. The independent components were then mapped using the mixing matrix and the indices formed prior to analysis. Each independent component and its PSD estimate were plotted with its spatial map for comparison.

4 RESULTS AND DISCUSSION

4.1 Method Optimization

Images were acquired with different echo times to determine optimal sensitivity to the low frequency resting state fluctuations previously seen in human studies. Previous studies have demonstrated the echo time dependency of the human resting state signal [47, 48]. Using seeds from comparable locations in SI chosen by the author, cross correlation maps were generated and compared visually for the best outcome. This TE dependency was similarly observed in the present animal data, in which a shorter echo time (TE=13 ms) improves the global signal-to-noise ratio and decreases the distortion seen in the image, but a longer TE (TE = 35 ms) provides more sensitivity to tissue specific T_2* effects. T_2* of the rat cortex at 11.7 T is about 25 ms, and typical BOLD-weighted studies use TEs in the range of 15-25 ms, depending on distortion and signal loss. Figure 4.1 below demonstrates that longer TEs allow better visualization of cross correlation despite signal loss.

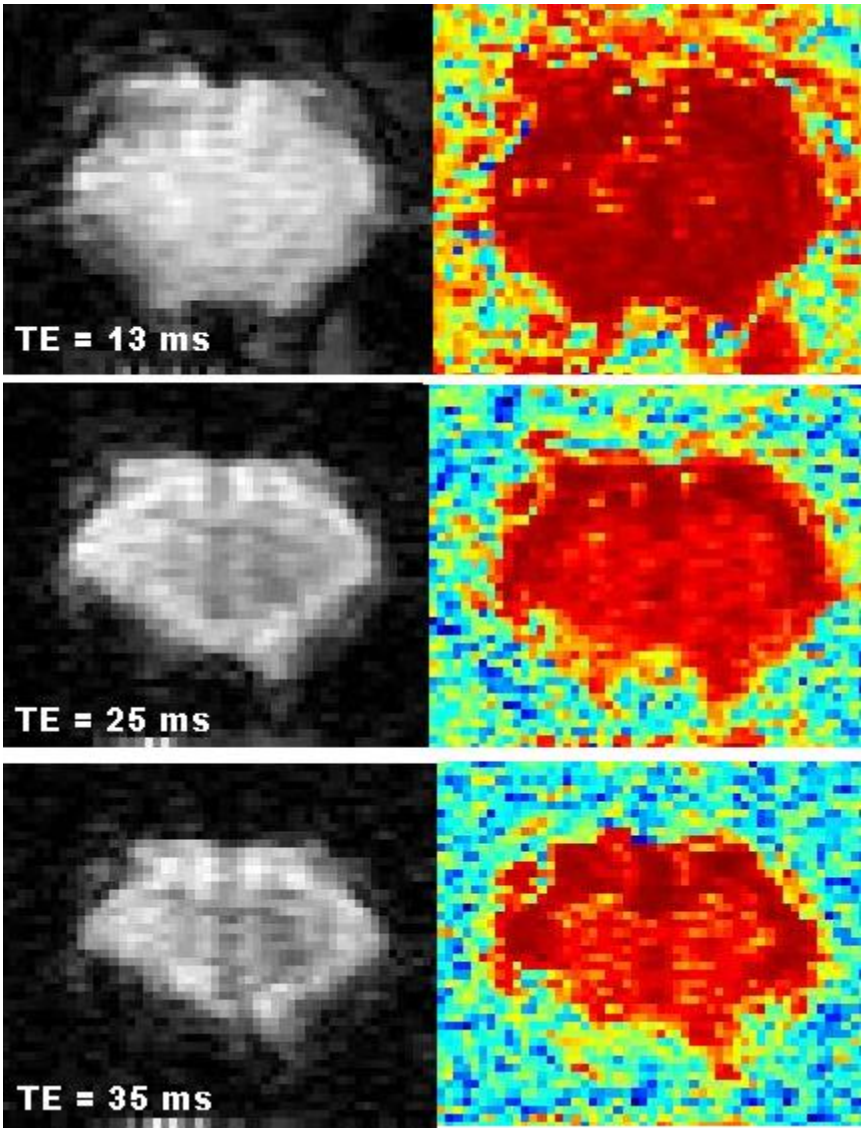

FIGURE 4.1 Signal loss vs. correlation gain with higher TE

Because the range in which spontaneous fluctuations may occur in the rat brain probably differs compared to that of the human brain, low-pass filter frequency cutoff was tested. To optimize visualization of activation in the cortex, a range of frequency cutoff values were used for the low-pass filter frequency (0.01-0.20 Hz) in cross correlation preprocessing. A frequency cutoff of 0.14 Hz was chosen to process images.

4.2 Alpha-chloralose Results

4.2.1 Power Spectral Density Estimation

The power spectra from the primary somatosensory cortex show structure in the low frequencies (<0.2 Hz) that is not present in the spectra of seeds chosen in the sagittal sinus or outside the brain. Peaks corresponding to respiration (~1 Hz) and cardiac pulsation (~4-5 Hz) can be seen in some spectra, particularly from the sinus. Figure 4.2 demonstrates the low frequency peaks found in SI. Figures 4.3 and 4.4 show the respiration and cardiac peaks found from power spectral estimation of areas of the brain outside SI.

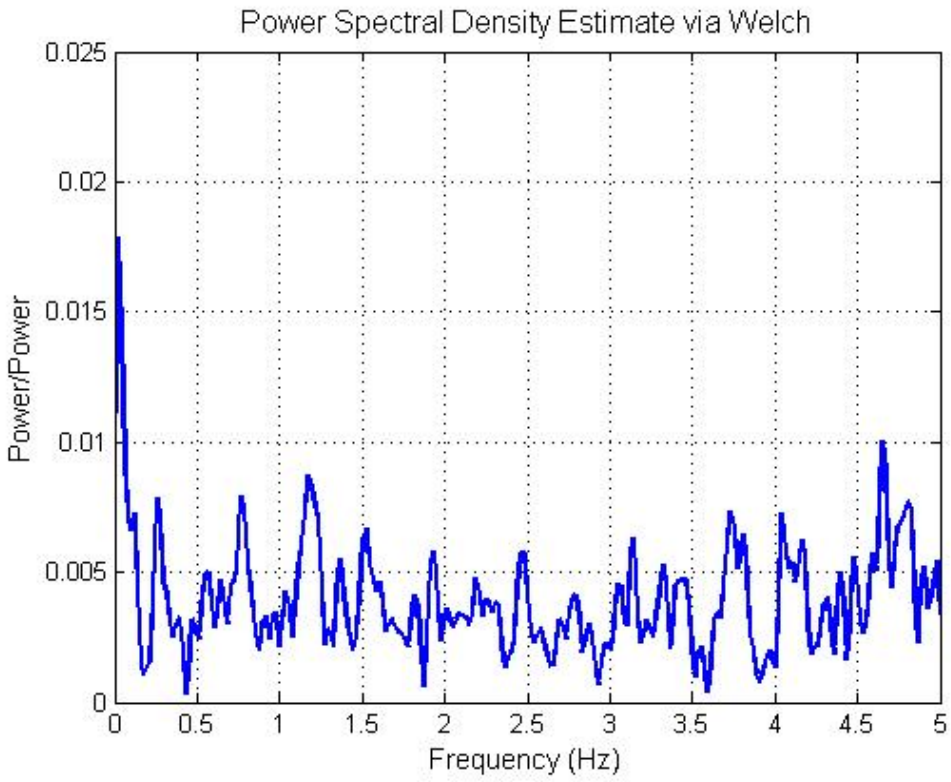

FIGURE 4.2: PSD of seed within SI showing low frequency peak

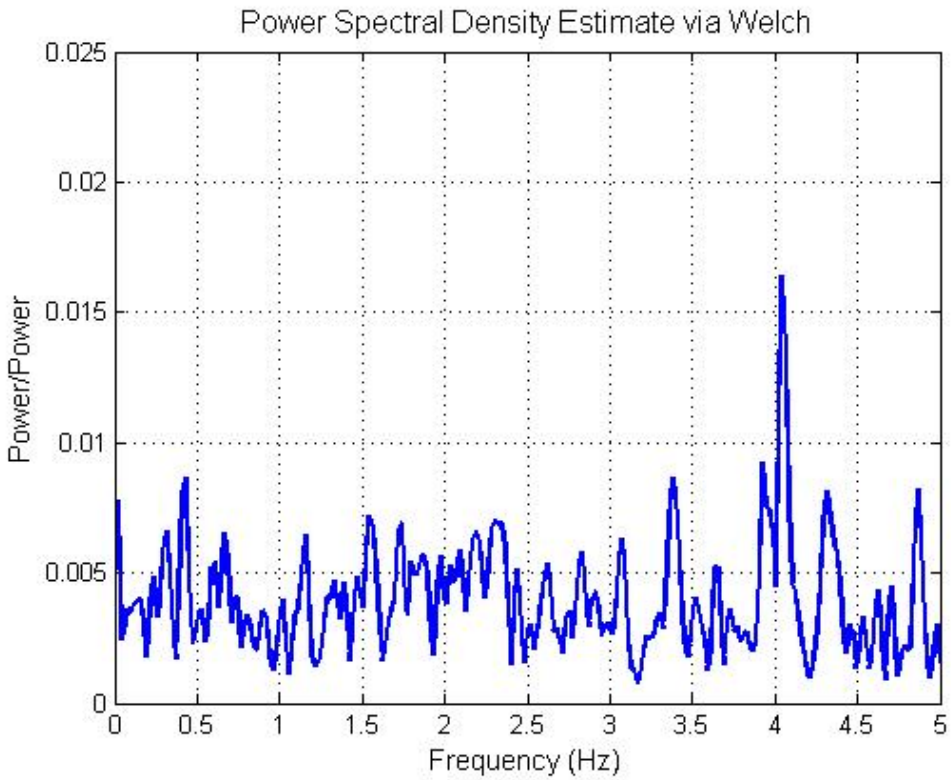

FIGURE 4.3: PSD of seed at the base of the brain. Note cardiac peak at ~4.3 Hz

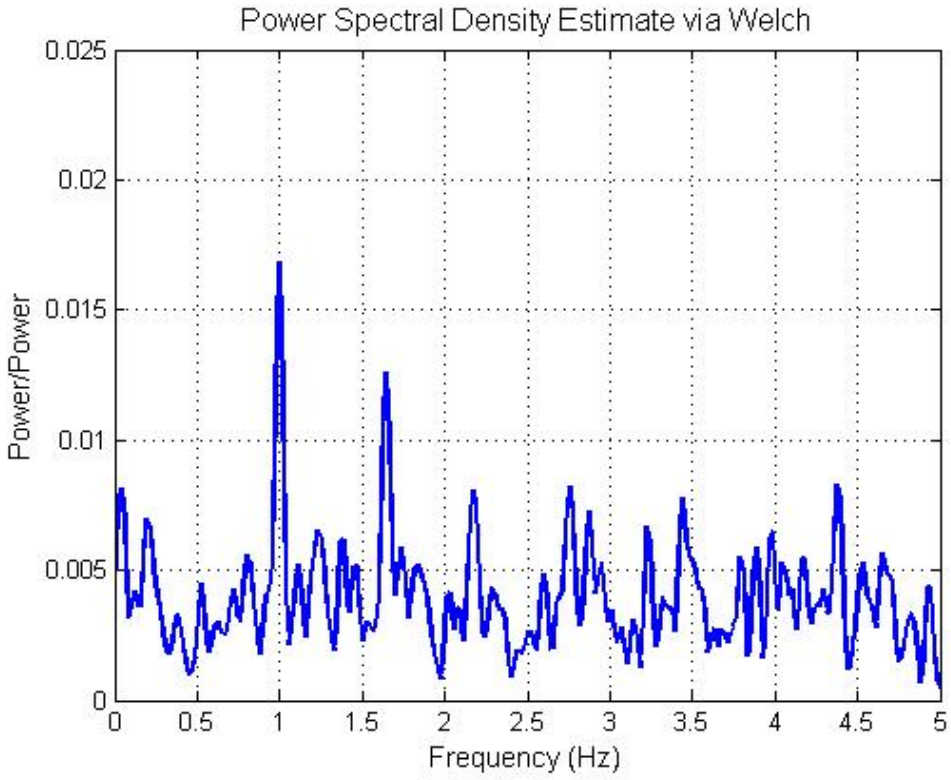

FIGURE 4.4: PSD of seed near ventricles of the brain. Note respiration peak at ~1 Hz

4.2.2 Cross correlation Analysis

Correlation maps demonstrate increased correlation in the cortex, especially in the primary and secondary somatosensory regions (average cc = 0.45 +/- 0.17), compared to subcortical structures (average cc = 0.07 +/- 0.14). Figure 4.5 below illustrates an anatomical image of the resting rat brain with the selected ROI for correlation indicated in yellow next to correlation map generated.

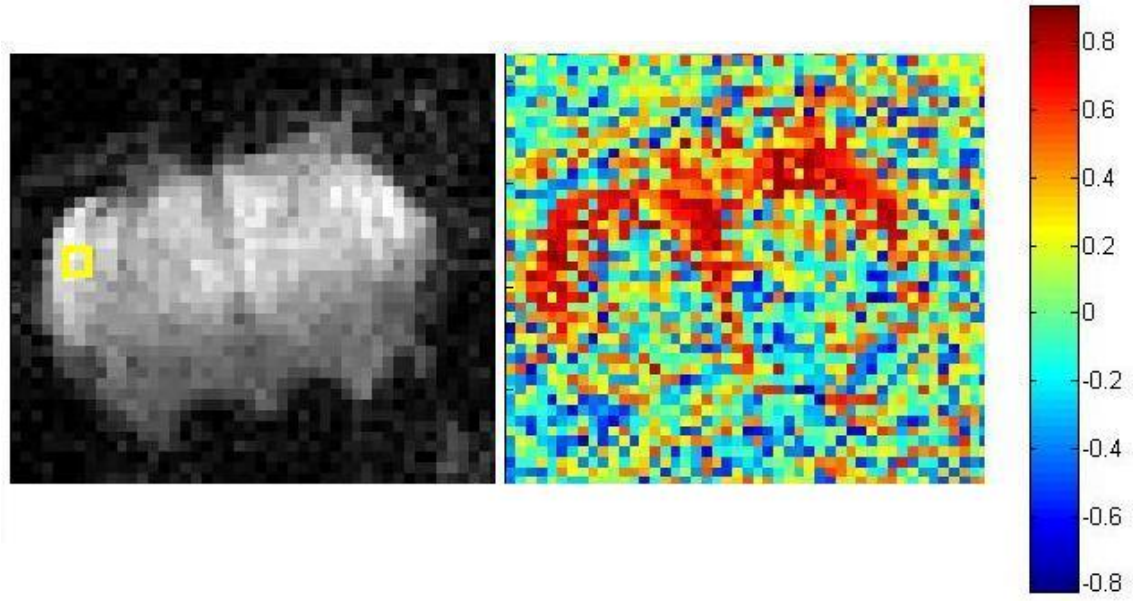

FIGURE 4.5: Anatomical Image from dataset and its corresponding correlation map. Yellow box on anatomical image indicates pixel seed chosen for CC map

Cross correlation values computed from a 4 x 4 ROI were taken and compared for all rat datasets. Cross correlation differences are statistically significant between the contralateral cortex and the contralateral subcortex for $P<0.01$, and between the

contralateral cortex and the ipsilateral subcortex for P<0.01. Figure 4.6 below shows the results of the t-test statistics for the combined rat data.

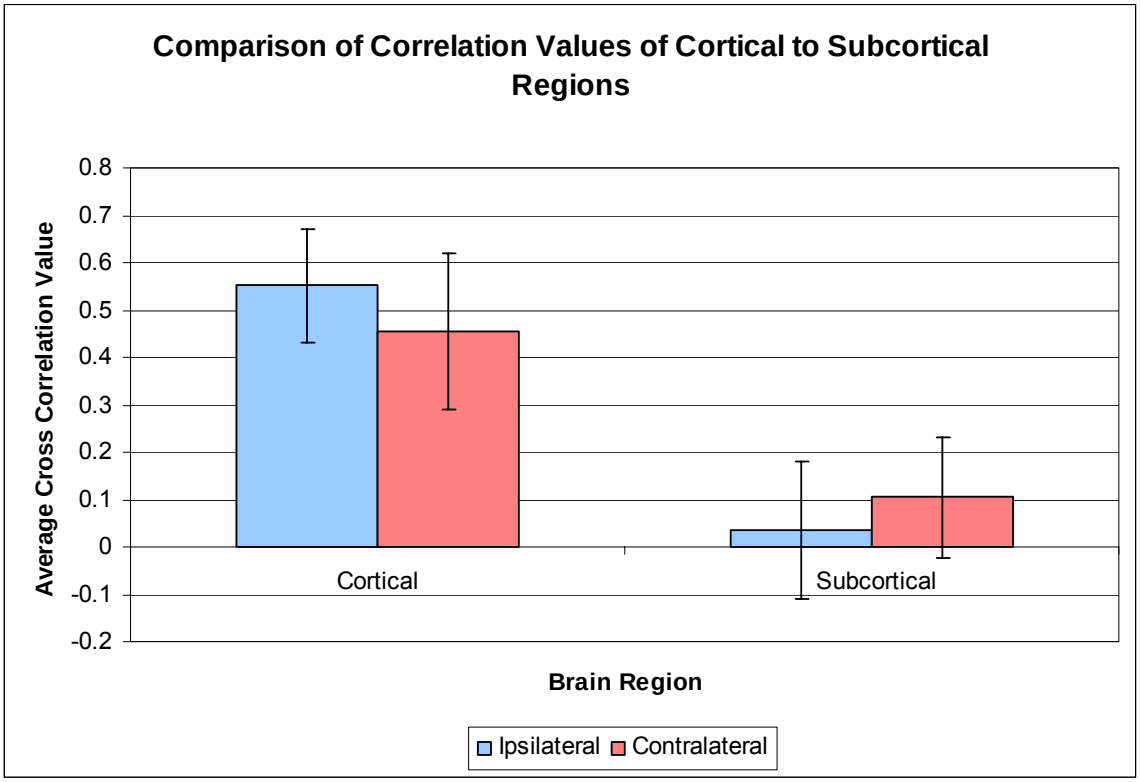

FIGURE 4.6: T-test data

Table 4.1 shows the data obtained from the cross correlation maps of the six rats. More than six datasets were used because of multiple scans, which indicate reproducibility of correlation in functional regions at rest.

Table 4.1: Averaged correlation coefficients within selected brain regions.

Rat	Ipsilateral Cortex	Contralateral Cortex	Ipsilateral Subcortex	Contralateral Subcortex	Average (subcortex)
1	0.587	0.524	0.1664	0.0519	
2	0.6171	0.5527	0.1312	0.1733	
3	0.6184	0.3393	0.2234	0.3669	
4	0.3046	0.3747	0.0249	0.0448	
5	0.6045	0.5576	-0.0327	0.0537	
6	0.6561	0.5796	0.0497	0.2113	
7	0.4787	0.5999	-0.2589	-0.1569	
8	0.6209	0.5958	0.0439	0.1945	
9	0.4514	0.4507	-0.0874	0.0344	
10	0.7131	0.0618	-0.1507	0.0415	
11	0.5609	0.5523	0.1568	0.0758	
12	0.4021	0.2657	0.1627	0.1567	
MEAN	**0.551233**	**0.454508**	**0.035775**	**0.103992**	**0.069883**
STDEV	**0.118094**	**0.165402**	**0.145844**	**0.128899**	**0.137371**

4.2.3 PCA and ICA

PCA was implemented to reduce the dimensions of the datasets. The principle components chosen for use in ICA explain 91 – 98% of the matrix variance, unless the dataset did not converge. In such case, the number of principle components chosen was reduced until convergence. Table 4.2 specifies the number of principle components used from each dataset and their combined percent variance.

TABLE 4.2 Principle Components and Explained Variance

Rat	Number of PCs chosen	Percent variance explained
1	6	91.7632
2	7	91.8046
3	10	94.0210
4	9	97.8225
5	5	90.6547
6	8	71.8409*

*Note procedure employed for non-convergence results in lower total variance explained

ICA of the resting state datasets results in the same number of independent components as principle components chosen to reduce dimensionality. Spatial maps of independent components whose PSD estimates show low-frequency structure correspond to the somatosensory cortex and strongly resemble cross correlation maps. Independent components that show low-frequency peaks in their power spectra and spatial maps correlating with SI show obvious low-frequency oscillation. Components whose PSD estimates show peaks in the 1 Hz region have spatial maps that correspond to ventricular regions of the rat brain. Sometimes several components show a peak in the region between 4 Hz and 5 Hz; spatial maps of these independent components correspond to the sinus, edges of the brain, and subcortical regions. Figure 4.7 shows the spatial map, the plotted independent component, and power spectrum corresponding to spontaneous fluctuations in the rat brain. Figure 4.8 illustrates plots and the spatial map with coherence in the ventricular regions. The power spectrum of this independent component peaks at ~1Hz. Figure 4.9 shows the spatial map associated with an independent component whose power spectrum shows a strong cardiac peak.

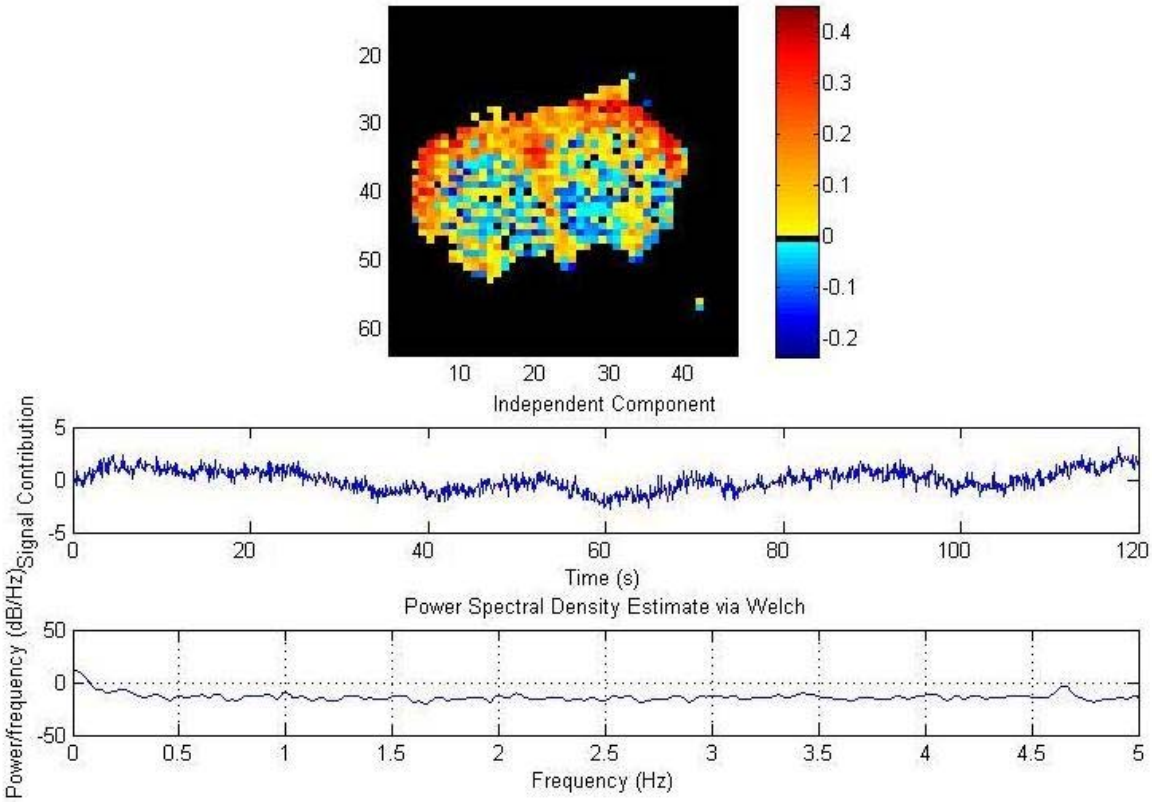

FIGURE 4.7 Independent component illustrating LFF

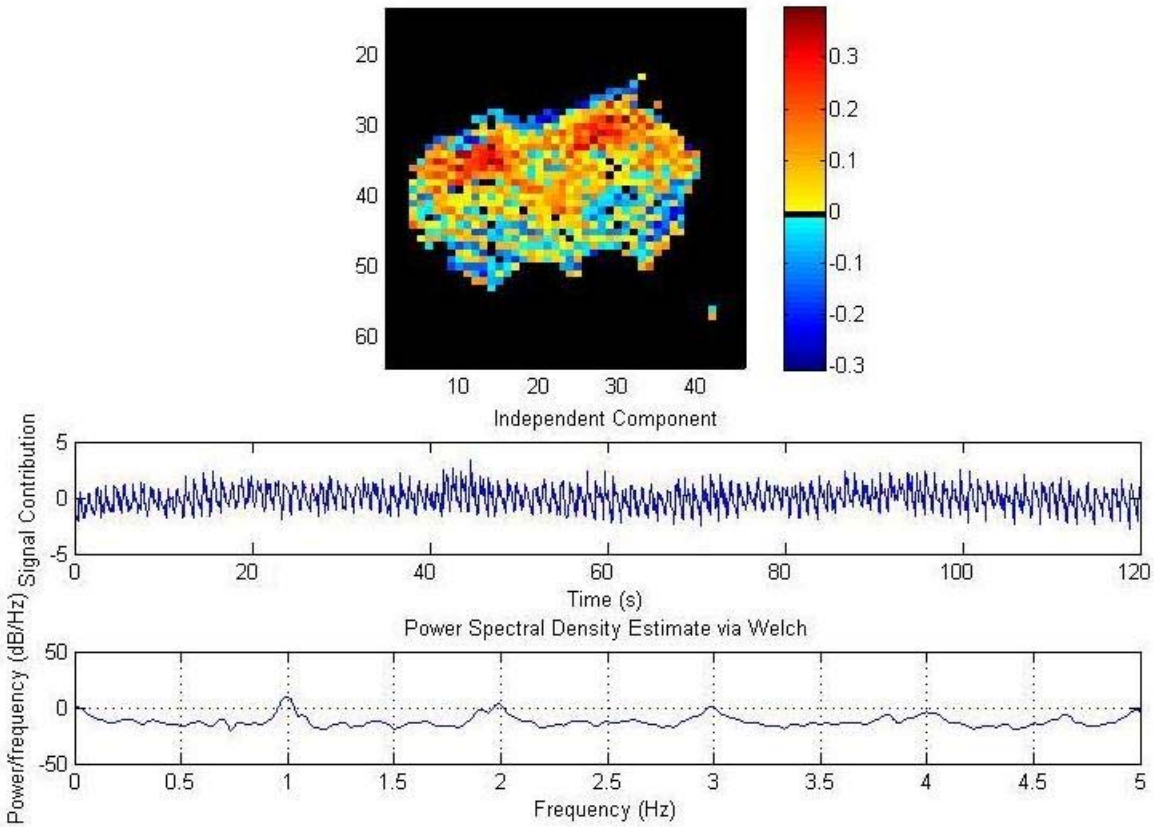

FIGURE 4.8 Independent component illustrating respiratory effects

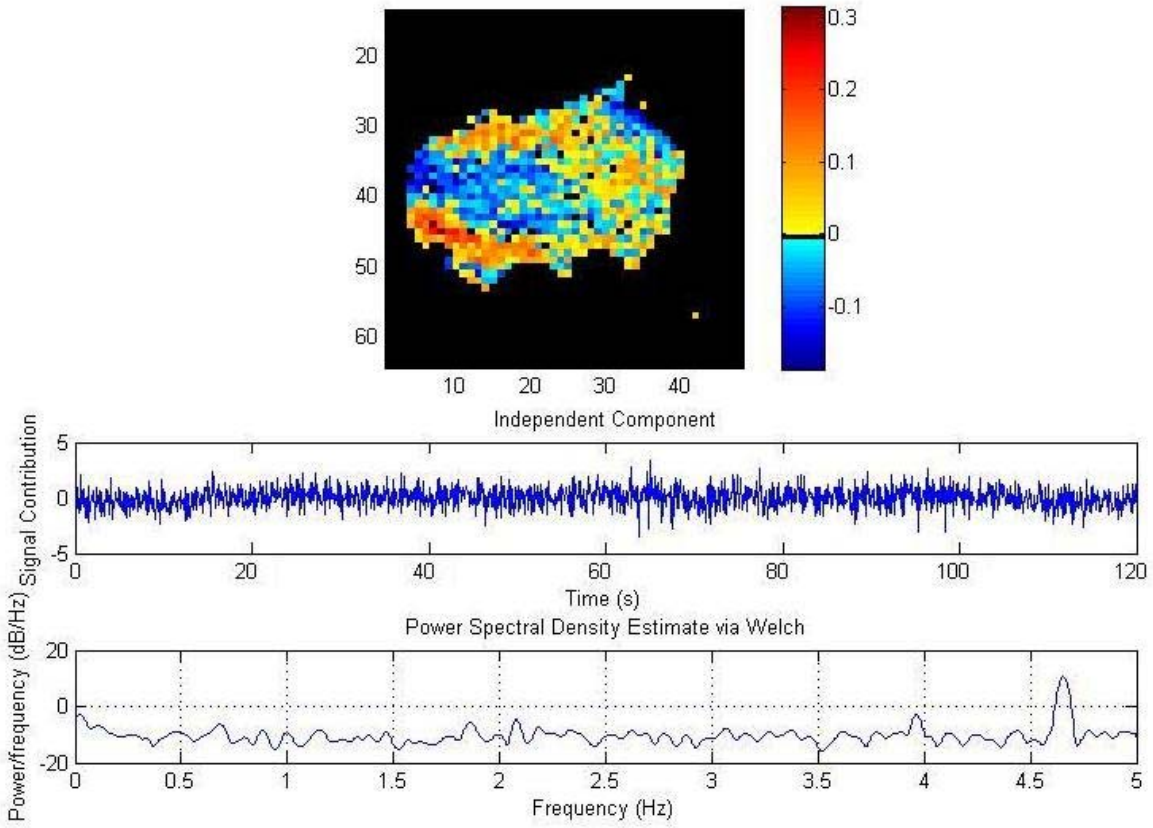

FIGURE 4.9 Independent component illustrating cardiac effects

The spatial maps associated with independent components whose PSD estimate had peaks in particular frequency regions, like 1 Hz for respiratory and 4-5 Hz for cardiac, do not always coincide with spatial regions in which one would expect movement or signal change for those particular frequencies. This could be interpreted in a number of ways, such as a significant change in hemodynamics during imaging that would affect unconventional areas, or gasping from anesthetics that may move the head despite constraints. Within these sets of independent components, there are still components that come from regions expected to have low frequency synchronicity. Occasionally, the only spatial map corresponding to power spectrum peak structure in the low frequencies

reveals correlation in the edges of the brain where draining veins are to be found. It is possible that some larger-scale hemodynamics, like draining veins, cannot be separated from low-frequency fluctuations and are actually contributors to the time course structure at all times. Independent component analysis is an ideal approach to answering questions such as these because of the possibility of multiple contributors to low-frequency fluctuations. The primary concern is to pin down the particular factors that are involved in spontaneous synchronous fluctuations due to neural activity. Figure 4.10 illustrates two more spatial maps attributable to low frequency fluctuations from other rats in the dataset.

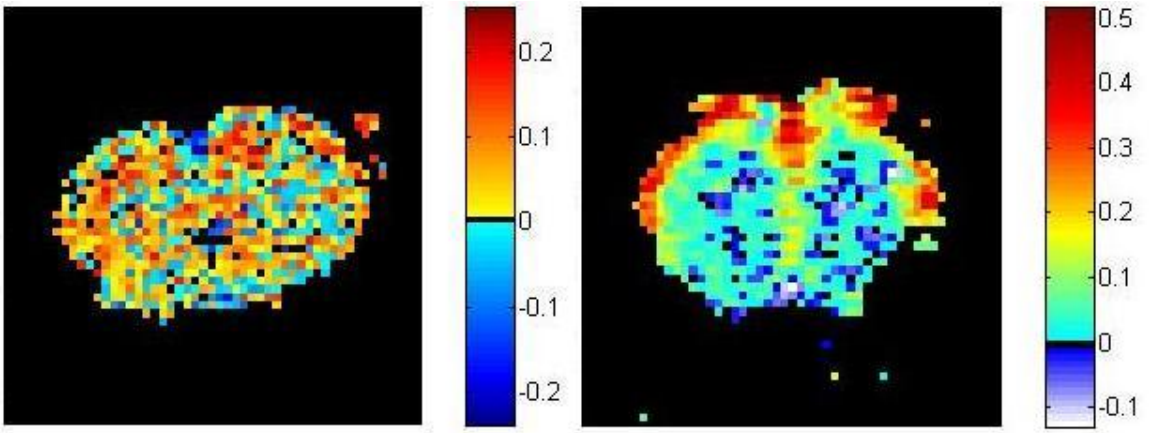

FIGURE 4.10 Low frequency fluctuations map to SI for multiple datasets

4.3 Isoflurane Results

Preliminary studies using isoflurane as an alternative anesthetic were conducted using a 9.4 T scanner. Cross correlation maps formed from seeds selected in SI do not yield correlations within only the somatosensory cortex. Low frequency peaks do not appear in the PSD estimates. Oscillations may be anesthesia level dependent [30]. In prior rodent fMRI experiments, BOLD responses have been shown to be reduced in the use

of isoflurane as compared to α-chloralose [49]. Another study shows that increasing concentrations of isoflurane that lead to loss of consciousness disrupt long-range antero-posterior phase synchronization of local field potentials rather than that in local anterior cortical areas [50]. Such impairment as measured with EEG could also manifest itself in resting state networks and be observed with fMRI.

Using FastICA to analyze a dataset, PCA was used to reduce the dimensions, as was used for the α-chloralose datasets. The distribution of the variance of each principle component was much more uniform than that of the α-chloralose datasets, as is illustrated in the PCA distribution shown in Figure 4.11.

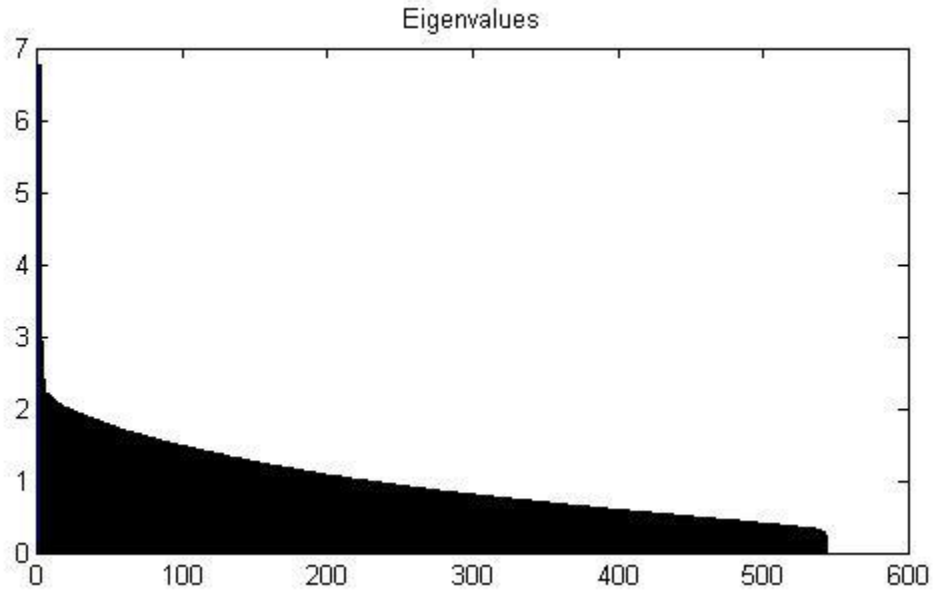

Figure 4.11: Principle components variance distribution of isoflurane data. Note more distributed variance values than is evident in alpha-chloralose data

Seven components were chosen arbitrarily to use for ICA. The maps of the resulting independent components seem to be evidence of lack of resting state synchrony in the isoflurane-anesthetized rats. No independent component shows low-frequency

fluctuation in the somatosensory cortex, while the components that were calculated do display physiological effects in appropriate locations. The PSD estimate of one independent component displays structure around 1 Hz, and its spatial map corresponds to ventricular regions in the brain. Figure 4.12 shows the imaging slice acquired in all datasets. Figure 4.13 illustrates the component with a strong 1 Hz contribution, which could be interpreted as respiratory artifacts.

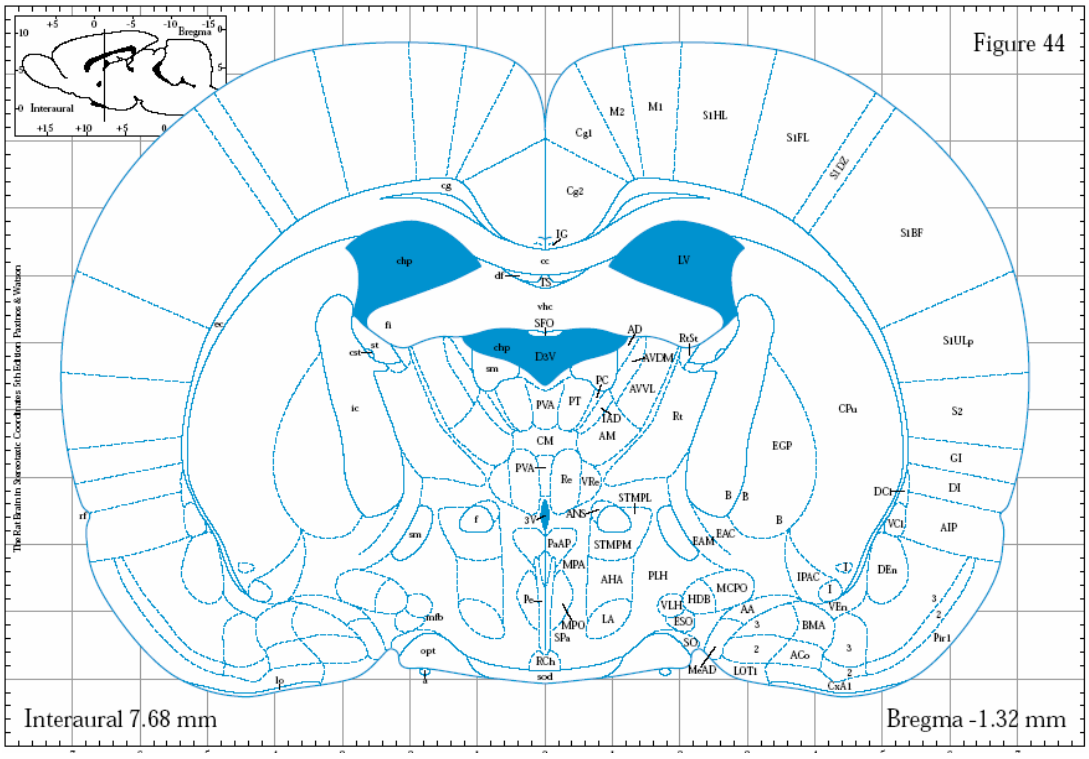

FIGURE 4.12: Paxinos Rat Brain Atlas of Imaging Slice. Note solid blue ventricles which correspond to the spatial map in the next figure [46].

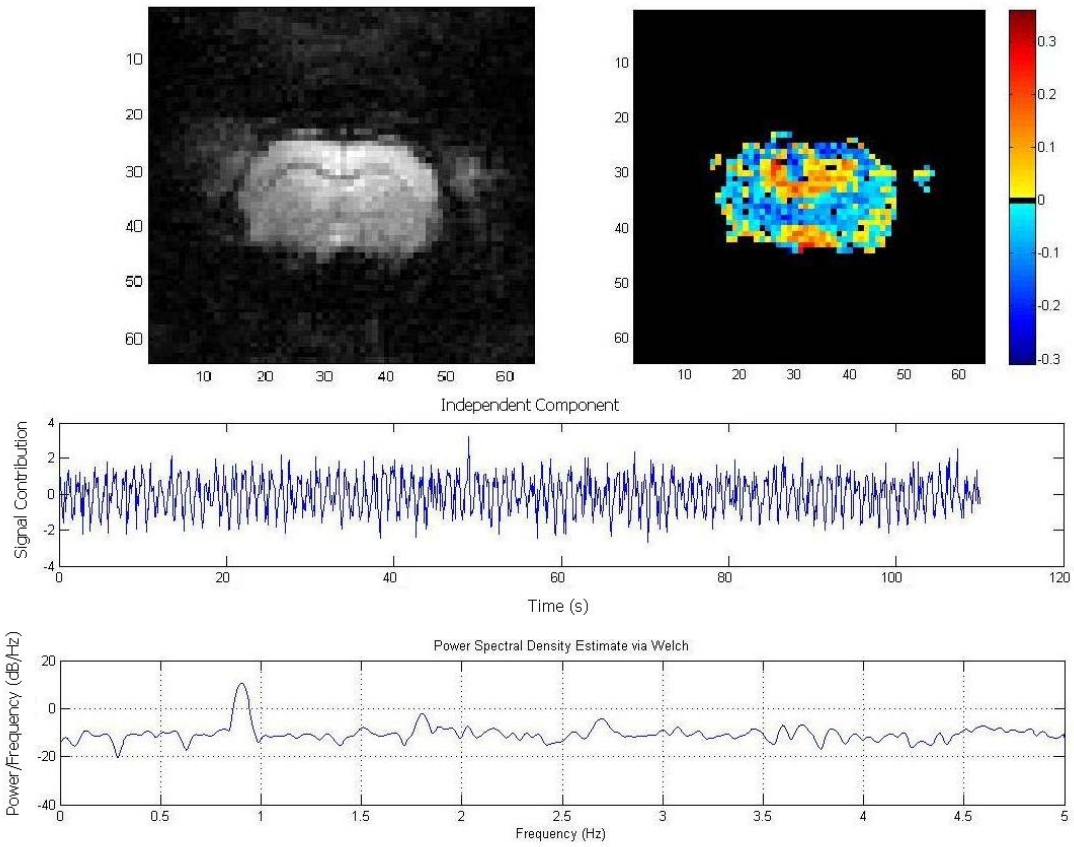

FIGURE 4.13 Image slice, spatial map, IC plot and PSD estimate exhibiting respiratory effects.

Another independent component spatially maps to the sinus, and its PSD estimate shows peak structure at about 0.05 Hz. Heart rate was not recorded for this series of imaging. Since there is no structure corresponding to the typical 4-5 Hz range for the heartbeat, it is possible that the Fourier transformation wrapped the cardiac peak around to the low frequency.

Attempts to obtain activation data through forepaw stimulation using isoflurane anesthesia have also proven unrewarding, but some groups have reported activation

detection using refined stimulation parameters and very specific combinations of isoflurane anesthesia [51].

5 CONCLUSIONS AND FUTURE WORK

Cross correlation, power spectrum estimation, principle component analysis, and independent component analysis each showed results that suggest resting state functional connectivity is a phenomenon that occurs in rats. Cross correlation maps reflect coherence between contralateral regions the somatosensory cortex based on a user-defined seed. Power spectrum estimation of time courses within the somatosensory cortex display peaks in the low frequencies that are not found outside SI or SII. Principle component analysis, when applied prior to independent component analysis, helps reduce the dimensions of large datasets to components that represent the majority of signal variance. Because the resting state BOLD signal fluctuation is only about 1% of the total imaging signal, one should keep in mind that dimension reduction with PCA may actually cut out the signal fluctuations associated with functional connectivity. Finally, independent component analysis separates the signals contributing to the overall MRI signal, which reveals system noise, physiological artifacts, and, most importantly, low-frequency fluctuations that correspond to the somatosensory cortex.

Such indications encourage further resting state network research with rats. More extensive use of promising data analysis techniques like independent component analysis will help better characterize the spontaneous fluctuations in the low frequencies. It will be useful to attempt ICA without reducing dimensions with PCA, which may allow better detection and further separation of low frequency components; also planned is

factor analysis and solely PCA with spatial maps. Additional studies planned for this investigation include varied image slice location and orientation, whole-brain imaging, and the use of alternate anesthetics that allow detection of synchronous frequency fluctuations.

After satisfactory LFF characterization is established, rats can be used as a human functional connectivity model. Electrophysiology and other invasive techniques can be used to investigate the physiological origins of resting state functional connectivity as well as decipher a more precise relationship between neural activity, metabolism, and blood flow. Understanding the origin of resting state connectivity has many implications for human studies because of the ongoing investigations that associate neuropathology and functional connectivity. In conclusion, this research indicates low-frequency fluctuations similar to those observed in humans do occur in rats during a resting state.

REFERENCES

1. Kiviniemi, V. *Low Frequency BOLD Fluctuations and Brain Functional Connectivity*. in *ISMRM*. 2006. Seattle.

2. Keilholz, S.D., et al., *Functional MRI of the rodent somatosensory pathway using multislice echo planar imaging.* Magn Reson Med, 2004. **52**(1): p. 89-99.

3. Bloch, F., *Nuclear induction.* Phys Rev, 1946(70): p. 460.

4. Purcell, E.M., H.C. Torrey, and R.V. Pound, *Resonance absorption by nuclear magnetic moments in a solid.* Phys Rev, 1946(69): p. 37.

5. Kumar, A., D. Welti, and R. Ernst, *NMR Fourier zeumatography.* J Magn Reson, 1975(18): p. 69.

6. Lauterbur, P., *Image formation by induced local interactions: Example employing nuclear magnetic resonance.* Nature, 1973(242): p. 190.

7. Mansfield, P. and A. Maudsley, *Fast scan proton density imaging by NMR.* J Phys E: Sci Instrum, 1976(9): p. 271.

8. Haacke, E.M., et al., *Magnetic Resonance Imaging: Physical Principles and Sequence Design*. 1999, New York: John Wiley & Sons, Inc. 914.

9. Ogawa, S., et al., *Brain magnetic resonance imaging with contrast dependent on blood oxygenation.* Proc Natl Acad Sci U S A, 1990. **87**(24): p. 9868-72.

10. Huang, W., et al., *Magnetic resonance imaging (MRI) detection of the murine brain response to light: temporal differentiation and negative functional MRI changes.* Proc Natl Acad Sci U S A, 1996. **93**(12): p. 6037-42.

11. Turner, R., et al., *Functional mapping of the human visual cortex at 4 and 1.5 tesla using deoxygenation contrast EPI.* Magn Reson Med, 1993. **29**(2): p. 277-9.

12. Babiloni, F., et al., *Multimodal integration of EEG, MEG and fMRI data for the solution of the neuroimage puzzle.* Magn Reson Imaging, 2004. **22**(10): p. 1471-6.

13. Madsen, P.L. and N.H. Secher, *Near-infrared oximetry of the brain.* Prog Neurobiol, 1999. **58**(6): p. 541-60.

14. Otte, A. and U. Halsband, *Brain imaging tools in neurosciences.* J Physiol Paris, 2006. **99**(4-6): p. 281-92.

15. Cho, Z.H., J.P. Jones, and M. Singh, *Foundations of Medical Imaging*. 1 ed. 1993, New York: John Wiley & Sons, Inc. 576.

16. Wong, E.C., R.B. Buxton, and L.R. Frank, *Quantitative imaging of perfusion using a single subtraction (QUIPSS and QUIPSS II).* Magn Reson Med, 1998. **39**(5): p. 702-8.

17. Aubert, A. and R. Costalat, *A model of the coupling between brain electrical activity, metabolism, and hemodynamics: application to the interpretation of functional neuroimaging.* Neuroimage, 2002. **17**(3): p. 1162-81.

18. Shulman, R.G., F. Hyder, and D.L. Rothman, *Biophysical basis of brain activity: implications for neuroimaging.* Q Rev Biophys, 2002. **35**(3): p. 287-325.

19. Friston, K.J., et al., *Value-dependent selection in the brain: simulation in a synthetic neural model.* Neuroscience, 1994. **59**(2): p. 229-43.

20. Biswal, B., et al., *Functional connectivity in the motor cortex of resting human brain using echo-planar MRI.* Magn Reson Med, 1995. **34**(4): p. 537-41.

21. Cordes, D., et al., *Mapping functionally related regions of brain with functional connectivity MR imaging.* AJNR Am J Neuroradiol, 2000. **21**(9): p. 1636-44.

22. Lowe, M.J., B.J. Mock, and J.A. Sorenson, *Functional connectivity in single and multislice echoplanar imaging using resting-state fluctuations.* Neuroimage, 1998. **7**(2): p. 119-32.

23. Gelnar, P.A., et al., *A comparative fMRI study of cortical representations for thermal painful, vibrotactile, and motor performance tasks.* Neuroimage, 1999. **10**(4): p. 460-82.

24. Friston, K.J., et al., *Functional connectivity: the principal-component analysis of large (PET) data sets.* J Cereb Blood Flow Metab, 1993. **13**(1): p. 5-14.

25. Kruger, G. and G.H. Glover, *Physiological noise in oxygenation-sensitive magnetic resonance imaging.* Magn Reson Med, 2001. **46**(4): p. 631-7.

26. Biswal, B.B., J. Van Kylen, and J.S. Hyde, *Simultaneous assessment of flow and BOLD signals in resting-state functional connectivity maps.* NMR Biomed, 1997. **10**(4-5): p. 165-70.

27. Kiviniemi, V., J. Ruohonen, and O. Tervonen, *Separation of physiological very low frequency fluctuation from aliasing by switched sampling interval fMRI scans.* Magn Reson Imaging, 2005. **23**(1): p. 41-6.

28. Mitra, P.P., et al., *The nature of spatiotemporal changes in cerebral hemodynamics as manifested in functional magnetic resonance imaging.* Magn Reson Med, 1997. **37**(4): p. 511-8.

29. Wada, Y., et al., *Interhemispheric EEG coherence in never-medicated patients with paranoid schizophrenia: analysis at rest and during photic stimulation.* Clin Electroencephalogr, 1998. **29**(4): p. 170-6.

30. Peltier, S.J., et al., *Functional connectivity changes with concentration of sevoflurane anesthesia.* Neuroreport, 2005. **16**(3): p. 285-8.

31. Cordes, D., et al., *Frequencies contributing to functional connectivity in the cerebral cortex in "resting-state" data.* AJNR Am J Neuroradiol, 2001. **22**(7): p. 1326-33.

32. Raichle, M.E., et al., *A default mode of brain function.* Proc Natl Acad Sci U S A, 2001. **98**(2): p. 676-82.

33. Gusnard, D.A. and M.E. Raichle, *Searching for a baseline: functional imaging and the resting human brain.* Nat Rev Neurosci, 2001. **2**(10): p. 685-94.

34. Fransson, P., *Spontaneous low-frequency BOLD signal fluctuations: an fMRI investigation of the resting-state default mode of brain function hypothesis.* Hum Brain Mapp, 2005. **26**(1): p. 15-29.

35. Greicius, M.D., et al., *Functional connectivity in the resting brain: a network analysis of the default mode hypothesis.* Proc Natl Acad Sci U S A, 2003. **100**(1): p. 253-8.

36. Fox, M.D., et al., *The human brain is intrinsically organized into dynamic, anticorrelated functional networks.* Proc Natl Acad Sci U S A, 2005. **102**(27): p. 9673-8.

37. De Luca, M., et al., *fMRI resting state networks define distinct modes of long-distance interactions in the human brain.* Neuroimage, 2006. **29**(4): p. 1359-67.

38. Fox, M.D., et al., *The BOLD onset transient: identification of novel functional differences in schizophrenia.* Neuroimage, 2005. **25**(3): p. 771-82.

39. Rombouts, S.A., et al., *Altered resting state networks in mild cognitive impairment and mild Alzheimer's disease: an fMRI study.* Hum Brain Mapp, 2005. **26**(4): p. 231-9.

40. Hayes, M.H., *Statistical Digital Signal Processing and Modeling*. First ed, ed. S. Elliot. 1996, New York: John Wiley & Sons, Inc.

41. Papoulis, A. and S.U. Pillai, *Probability, Random Variables, and Stochastic Processes*, ed. S.W. Director. 2002, New Delhi: Tata McGraw-Hill Publishing Company Limited. 852.

42. Kiviniemi, V., et al., *Comparison of methods for detecting nondeterministic BOLD fluctuation in fMRI.* Magn Reson Imaging, 2004. **22**(2): p. 197-203.

43. Calhoun, V.D. and T. Adali, *Unmixing fMRI with independent component analysis.* IEEE Eng Med Biol Mag, 2006. **25**(2): p. 79-90.

44. Hyvarinen, A. and E. Oja, *Independent component analysis: algorithms and applications.* Neural Netw, 2000. **13**(4-5): p. 411-30.

45. Calhoun, V.D., et al., *Spatial and temporal independent component analysis of functional MRI data containing a pair of task-related waveforms.* Hum Brain Mapp, 2001. **13**(1): p. 43-53.

46. Paxinos, G. and C. Watson, *The Rat Brain In Stereotaxic Coordinates*. Fifth ed. Vol. 1. 2005, London: Elsevier Academic Press.

47. Hyde, J.S. and B. Biswal, *Functionally related correlation in the noise*, in *Functional MRI*. 2000, Springer-Verlag: Berlin. p. 263-275.

48. Peltier, S.J. and D.C. Noll, *T(2)(*) dependence of low frequency functional connectivity.* Neuroimage, 2002. **16**(4): p. 985-92.

49. Liu, Z.M., et al., *Imaging oxygen consumption in forepaw somatosensory stimulation in rats under isoflurane anesthesia.* Magn Reson Med, 2004. **52**(2): p. 277-85.

50. Imas, O.A., et al., *Isoflurane disrupts anterio-posterior phase synchronization of flash-induced field potentials in the rat.* Neurosci Lett, 2006. **402**(3): p. 216-21.

51. Masamoto, K., et al., *Relationship between Neural, Vascular, and BOLD Signals in Isoflurane-Anesthetized Rat Somatosensory Cortex.* Cereb Cortex, 2006.